Morphological Analysis of Galaxies

A thesis submitted to the

University of Calicut, Kerala for the award of the

Degree of **DOCTOR OF PHILOSOPHY**

in **PHYSICS**

under the Faculty of Science

by

Dhanya Joseph

Department of Physics

University of Calicut

Kerala, India

May 2016

"Equipped with his five senses, man explores the universe around him and calls the adventure Science."

—Edwin Hubble, Astronomer

Dedicated to my Parents

CERTIFICATE

This is to certify that the thesis entitled "**Morphological analysis of galaxies**" submitted to the Department of Physics, University of Calicut by **Mrs. Dhanya Joseph** in partial fulfilment of the requirements for the award of the degree of **Doctor of Philosophy** is the original work carried out by her under my supervision and guidance at the Department of Physics, University of Calicut. This thesis has not been submitted by her for the award of any other degree, diploma, associateship, fellowship etc. of any university or institute.

Dr. C. D. Ravikumar
Supervisor
Department of Physics
University of Calicut

DECLARATION

I hereby declare that the work presented in this thesis is based on the original work done by me at the Department of Physics, University of Calicut under the supervision of Dr. C. D. Ravikumar. This thesis has not been submitted by me for the award of any other degree, diploma, associateship, fellowship etc. of any university or institute.

Date: 02-03-2018   **Dhanya Joseph**

Department of Physics

University of Calicut

Contents

List of Tables

List of Figures

Acknowledgement

List of Publications

• Journals

1. **Dhanya Joseph**, C. D. Ravikumar and A. U. Preetha
   "Structural analysis of early-type galaxies-Near IR observations", *International Journal of Scientific and Engineering Research*, **5**, 03, 2014.

2. **Dhanya Joseph**, C. D. Ravikumar and A. U. Preetha
   "Disks in Early-Type Galaxies from NIR observations", *Research Journal of Recent Science*, **3**, 420-422, 2014.

3. **Dhanya Joseph**, C. D. Ravikumar, A. U. Preetha and M. Nikesh
   "Structural Properties of early type Galaxies with Ionised Gas", *Research Journal of Physical Science*, **1(5)**, 7-10, 2013.

4. **Dhanya Joseph** and C. D. Ravikumar
   "structural studies of early-type galaies in Mid-IR observations", **In Preparation**.

Abstract

The main objective of this thesis is to study the morphology of early-type galaxies in the nearby (z <0.02) universe. We also aim to learn more about the formation and evolution of such galaxies. The sample contains 65 galaxies with 45 ellipticals and 20 lenticulars. Most of the sample galaxies reside in field or low density environment. The near infrared and mid-infrared observations were used in this study. J (1.25 μm) and K (2.16μm) band images of NIR observations were obtained from Two Micron All Sky Survey (2MASS). 3.6 μm images of mid-IR observations were obtained from Spitzer Science Survey. The structural information of galaxies was studied by isophotal profile fitting method and two dimensional bulge disc decomposition method. Recent studies as the field of structural analysis of galaxies suggest that the most suitable method for structural studies is the two dimensional bulge disc decomposition. The light profiles of bulge and disc components were modelled by Sérsic functions and exponential functions respectively. From the NIR image analysis, we obtained lesser value of Sérsic index for all the galaxies. We also found that the galaxies had a significant disc component. The correlations between different structural parameters are studied. Larger galaxies were found to be more luminous and had fainter mean surface brigthness. The disc scale length was correlated with disc luminosity and also with the central disc surface brightness. The disc scale length was positively correlated with bulge effective radius. This relation strongly suggests that the bulges present in the galaxies were formed from already existing discs. As the 2MASS images were shallow, we have also employed mid-IR data from the Spitzer space telescope, with better sensitivity, to explore the findings obtained in the 2MASS image analysis. The Spitzer data analysis also supported results obtained from 2MASS with more accurate results. From the relation of Sérsic index and B/T ratio, we point out that two categories of bulges could be present in the

sample. A class of galaxies with lower values of Sérsic index (n <2.5) support the presence of pseudobulges and higher value of Sérsic index (n >2.5) of galaxies support the presence of classical bulges. We conclude with the finding that significant amount of disc component is present in our sample galaxies including ellipticals. The relations of structural components exhibited by these galaxies were different as their bulges were different in nature.

Chapter 1

Introduction

Galaxies are considered as the building blocks of the universe and include collection of stars, dust and gas bounded by gravitational force. Finding answers to fundamental queries about galaxies such as shape, type, formation scenarios eventually lead to the scientific exploration and advancement in the galaxy studies. Science progressed well in observational astronomy with advanced high resolution telescopes along with effective image analysis techniques. In this thesis, we focus on the morphological studies of galaxies observed in near infrared and mid infrared wavelengths.

1.1 Development of studies on galaxies

In astronomy, noticeable development on studies about gaaxies happened around 17th century. The word 'galaxy' and 'Milky Way' had their origin in Greek and Latin mythology. On a moonless night of summer and winter sky, a band of light appeared milky and due to the milky appeerence of this band it was called as Milky Way. In 1610, Galileo observed the Milky Way and discovered that, the luminous band of light consisted of huge number of stars that could not be resolved by naked eye. In mid eighteenth century Immanuel Kant published his observations about the planar structure of the Solar System and the ordered rotation of planets without collapse. He also pointed out that the Milky Way may not be the only stellar system. Some of the nebulae which appear as elliptical patches of light seen in the sky might

also be similar in structure to Milky Way galaxy (Binney & Merrifield, 1998). The discovery of the spiral nebulae by W. Parsons in 1845 was another important stage in the field of astronomy. Discussions about the Milky Way galaxy also happened during that period. In 18th century, systematic studies of nebulae were started by the use of powerful telescopes of that time. At the end of 18th century, Charles Messier compiled a catalogue called Messier Catalogue (M) with 109 bright nebulae in the northern sky. William Herschell and his sister studied the entire sky, and compiled a catalogue known as the General Catalogue (GC) of nearly 5000 nebulae in 1864. In 1888, Dreyer introduced the New General Catalogue (NGC) and Index Catalogue (IC) in 1895. Succeeding centuries were building stages of astronomical studies with development of better and bigger telescopes. At the end of 19th century photography was used in astronomy. By long exposure of photographic plate it was possible to observe very faint objects that were not accessible visually. This development initiated steps towards the quantitative astronomy (Binney & Merrifield, 1998). The technological developments of computer was the next stage of astronomical study. Invention of computers was very much useful for astronomers to handle large quantity of data and their analysis. The development of charge coupled devices (CCDs) replaced the photographic plate as light detector (Binney & Merrifield, 1998). These advanced technology was beneficial to improve the quality of observed image. CCDs were more efficient than photographic plate, and even detected the outer faint part of galaxies. In 20th century it was believed that, our galaxy possessed a disc like structure with sun as one of the main component situated near to its centre.

Extra galactic astronomy is the branch of astronomy that focuses on the study of objects outside our Milky Way galaxy. The nature of external galaxies was confirmed by the measurment of large radial velocity of stars compared to the stars in Milky Way.

1.2   Classification of galaxies

In 1920, Hubble used the 100-inch telescope placed at Mount Wilson Observatory, USA, to make several observations and analysis. Many important findings such as

the presence of individual stars in M31 and M33 were given by him, and also identified the presence of Cepheid variable stars and Novae (Hubble & Sandage, 1953). These findings lead towards the possibility of the presence of group of stars outside the Milky Way. Based on the apparent shape and structure, Hubble proposed the classification scheme called morphology. In 1925, he introduced the concept of the tuning fork diagram to classify the extra galactic nebulae based on the size of the bulge present in the system (Hubble, 1926). By this type of classification he proposed an evolutionary sequence of early-type (ellipticals) to late-type (spirals) systems. The classification scheme was published in his book *'The Realm of the Nebulae'* (Hubble, 1936). Like most astronomers, our study is also based on the well known classification scheme of Hubble's tuning fork diagram as shown in Figure 1.1. The widely accepted classification scheme also known as the Hubble's classification, was developed by the visual appearance of galaxies and is qualitative in nature. Based on this classification, Hubble suggested that galaxies evolved from the left hand side of this sequence to the right. The galaxies on the left end of the sequence were called early-type galaxies and the right hand side were reffered to as late-type galaxies. Galaxies placed at the left hand side of the turning-fork diagram were smooth and structureless. Shape of these galaxies vary from round to highly elongated form. These galaxy types were designated as En, where n is an integer describing the apparent axial ratio (b/a). The integer n close to $n = 10[1 - (b/a)]$, where b/a is the apparent axial ratio, *a* is the major axis and *b* the minor axis of the galaxy. According to the value of integer n, elliptical galaxies were designated from E0 to E7. E0s were circular where as E7s were the most elongated elliptical galaxies. After the elliptical galaxies, Hubble's diagram bifurcates into two branches called normal and barred galaxies. In the middle of Hubbles turning-fork diagram, the class of galaxies known as lenticular galaxies were designated as S0 or SB0 based on the presence of a bar feature. The S0 galaxies were characterised by smooth central surface brightness condensation called 'bulge' or 'spheroidal component', similar to an elliptical galaxy and surrounded by a large region of less steeply declining brightness called disc. In the Hubble's sequence, lenticular galaxies were followed by the spiral galaxies. The normal spiral galaxies contained a central brightness condensation similar to an elliptical galaxy situated at the center and the outer disc contains spiral arms. Barred spiral galaxy contained a spiral arm, a bar and often with dark

lense, produced by the absorption of light by dust. The normal spirals and barred spirals contain subtypes based on the relative importance of central spheroidal component and the outlying disc that produced the total light distribution in a galaxy. It also depends on the tightness of spiral arms are wound and degree to whic the spiral arms are resolved into stars and individual emission nebulae (Binney & Merrifield, 1998). Early-type spirals contained conspicuous bulge and tightly wound spiral arms designated as Sa or SBa. SBa are barred spirals and Sa are not. Late type spirals contained small central bulge and loosly wound and highly resolved arms. They were represented as Sc and SBc. In between Sb and SBb were situated.

The fourth group of galaxies were unsymmmetrical and were assigned to two classes of irregular galaxies(Irr I and Irr II) as represented in the right hand side of the diagram.

Hubble tuning fork diagram was advantageous due to its easiness of use and simplicity to understand. However, major drawback was that, the classification did not include few of the galaxies like dwarf ellipticals (dE), cD galaxies that are giant ellipticals normally seen in the centre of the clusters, star burst galaxies, interacting and merging galaxies etc. In order to overcome the drawbacks, modifications to the classification scheme were made by several researchers (Kormendy & Bruzual A., 1978; Kennicutt, 1981; Dressler, 1980, 1984). The well known extension was proposed by de Vaucouleurs (1991) and created morphological details available in the Second Reference Catalogue (RC2) and later the Third Refrence Catalogue (RC3). A special class of galaxies were included in the Hubble's classification by Sandage & Visvanathan (1978). However, despite such modifications, it is still the Hubble classification that is widely used.Some of the general properties of early and late type systems are mentioned below.

Early type galaxies include elliptical and lenticular galaxies, mainly with uniformly old and red population (Tantalo et al., 2010). It was defined by the homogeneous class of objects and was formed at high redshift (Bressan et al., 1994). They contained negligible amounts of gas and very little star formation (Bressan et al., 1994).

Elliptical galaxies

Elliptical galaxies are considered as featureless, smooth with elliptical shape in photographs and as very quiet systems (Abhyankar, 1992). These were devoid of interstellar dust, cool gas and young blue stars (Jiang et al., 2011). Elliptical galaxies show smooth variations of intensity across the disc. Most of the stars present in elliptical galaxies were found old and would have formed at earlier epochs.

Lenticular galaxies

Lenticular galaxies, are considered as the transition type between the ellipticals and spirals (Binney & Merrifield, 1998). The brightness varied like ellipticals in the inner part and exponentially like spirals in the outer parts. Three classes of lenticulars were present, such as $S0_-$, $S0$ and $S0_+$. $S0_-$ are similar to ellipticals, $S0$ with flat ring at the periphery and $S0_+$ with the presence of spiral arms.

Spiral galaxies

Spiral galaxies are considered as late type galaxies that contain central brightness condensation resembling an elliptical, located at the centre of a thin disc with spiral arms.

Irregular galaxies

These types of galaxies had no specified structure or lack dominant nucleus and rotational symmetry. This can be divided into two classes: First with resolved OB stars and emmision nebulosities like Magellanic clouds known as Irr I. The second one (Irr II) are irregular galaxies with amorphous structure.

One of the fundamental and easily accessible physical parameters of galaxies was its morphology. Morphological studies of galaxies lead to understanding scenarios of formation, evolution, star formation rate etc. The first attempt of classification of galaxies based on their morphology was done by Edwin Hubble as described in Section 1.2.
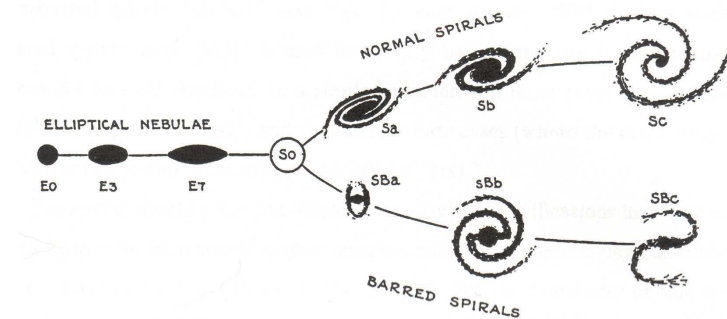
Figure 1.1: Hubble Classification of galaxies from early to late type systems

1.3 Surface Photometry

Surface photometry was the oldest method introduced first by Reynolds (1913) to study quantitatively the two dimensional light distribution of galaxies, like extended objects in the sky (de Vaucouleurs, 1948; Fish, 1964; Freeman, 1970; Milvang-Jensen & Jørgensen, 1999). This structural analysis and their correlations could guide to understand the formation and evolution of various galaxies. The image of galaxy can be described by more than one quantity like size, luminosity, magnitude, ellipticity, etc. So the quantitative analysis of galaxies would be essential to study the structure, formation and evolution. Earlier the surface photometry was done by the use of photographic plate detectors. But due to the low quantum efficiency, non-linearity and narrow dynamic range detection, this technique had lesser accuracy. The sky brightness and atmosphere turbulence also affect the galaxy brightness distribution. It was a time consuming process and required the user interaction for image processing. At this digital era, the charge coupled devices (CCD) could overcome these difficulties and enable the detection of the fainter light also. The advances in the surface photometry technique can be used to reduce the two dimensional (2D) image data into one dimensional (1D) surface brightness profile. The development of computer language and processing power, simplified many of the problems. Now it is possible to reduce numbers of galaxies in lesser time. However, galaxies are not uniform in their appearance, and forcing the reduction of their light distributions often leads to a loss of potentially valuable information (Schombert & Smith, 2012). Selection of a suitable profile to describe the galaxy would not be an easy task. The

first largest sample of galaxies was studied quantitatively for the morphology by Dressler (1980) with about 6000 galaxies in 55 clusters. Mainly two types of fitting methdes were available, one dimensional and two dimensional. One dimensional method was simple, fast and works in low S/N conditions. The major or minor axis profiles was fitted by use of one or more components or it was an azimuthally averaged surface brightness profile of the galaxy. The profile extracted along the major axis of a galaxy drops many of the information in the image (Rauscher et al., 1998). In this case minor axis profiles were also essential, as the bulge dominates the profile along this axis. In two dimensional profile fitting, information in the whole image were used to build a model for each component and thus differences in the projected ellipticities and position angles become an advantage (de Souza et al., 2004). Two dimensional fitting considered the nonaxisymmetric components also. Compared to one dimensional method two-dimensional method was more reliable (de Jong, 1996a).

The basic information of an astronomical object can be measured as the magnitude and luminosity. Usual method to measure the magnitude of astronomical object is the aperture photometry (de Vaucouleurs, 1977). Galaxies are extended objects and to choose the correct aperture for a galaxy is a main problem. If the size of aperture was large compared to the galaxy size, then it would produce noise from the sky and also from the nearby sources to the total flux of the galaxy. Another significant issue is the fixed surface brightness threshold which also would affect the flux measurement. Hence surface photometry is the better photometric method for the structural analysis of galaxies.

1.4   Surface brightness profiles

The light distribution of galaxies was described by surface brightness profiles. Surface brightness profile is of importance in the galaxy classification studies, which leads to the better understanding of galaxy formation scenarios. It could be explained as the intensity fall off of a model away from the peak controlled by the

model profile function (Peng et al., 2010).

Some of the surface brightness profiles used in surface photometry were major and minor axis profiles (Michard, 1985), azimuthally averaged profile (van der Kruit, 1987) and equivalent profile (Blackman et al., 1979). These methods were good, simple and can be easily accessible even at low signal to noise (S/N) conditions. However, besides advantages it had limitations. The varying ellipticity and position angle of isophotal fitting makes it difficult to define the profile correctly. The presence of non axi-symmetric components, if any, in the galaxies also could not be identified correctly (Wadadekar et al., 1999). Instead of 1D method (see Section 1.3), two dimensional method would be more accurate (de Jong et al., 2004). In structural studies of galaxies 2D method was more better (Fisher & Drory, 2008; Gadotti, 2009; Peng et al., 2002). The main advantage of 2D fitting is that it uses whole image for model fitting and thus each pixel of the images could be used for the study (Byun & Freeman, 1995). 2D fitting method, modelled every component in a galaxy and considers the non axi-symmetric parameters also. de Jong (1996b) studied both 1D and 2D model fitting and suggested that 2D as more accurate than 1D. Different algorithms of 2D decompostion were used by different researchers to address specific problems like studies on face-on spiral galaxies, barred galaxies, distant galaxies, modelling additional components present in a galaxy etc (de Souza et al., 2004; Simard, 1998; Wadadekar et al., 1999; Gadotti, 2008; Laurikainen et al., 2005; Peng et al., 2002). In our studies we used the Sérsic and exponential profiles for defining the bulge and disc components respectively.

1.5   de Vaucouleurs profile

The light distribution in galaxies could be studied by mathematical functions. High degree of regularity of surface brightness distribution in elliptical galaxies could be usually modelled by the classical de Vaucouleurs law (de Vaucouleurs, 1948, 1953).

$$I\left(R\right) = I_e \exp\left(-7.67\left[\left(\frac{R}{R_e}\right)^{\frac{1}{4}} - 1\right]\right) \tag{1.1}$$

Where $I(R)$ is the intensity at radius R, R_e is the radius of the circular aperature that contained half of the total light of the galaxy as called effective radius and I_e is the intensity at this radius. de Vaucouleurs law can be more suitable for brightest elliptical galaxies in the cluster. The inner region of the giant elliptical galaxies could be modelled well by de Vaucouleurs law, but the outer regions with enhanced light could only be poorly modelled. Several objects including the bulges in late type galaxies could not be defined correctly by de Vaucouleurs law. Hence Jose Sérsic (Sérsic, 1963; Sersic, 1968) generalised the de Vaucouleurs $r^{1/4}$ law to $r^{1/n}$ law. The structural studies of different samples of single and multicomponent fitting done by many of the researchers reported that Sérsic profile would be more accurate for defining the isophote of early-type galaxies (Caon et al., 1993; Andredakis et al., 1995; de Jong, 1996b; Graham, 2001; Gadotti, 2009). In this thesis we used the Sérsic law.

1.5.1   Sérsic profile

The Sérsic function is described as,

$$I(R) = I_e \exp\left(-b_n \left[\left(\frac{R}{R_e}\right)^{\frac{1}{n}} - 1\right]\right) \tag{1.2}$$

where R_e is the effective radius, I_e is the intensity at this radius. The quantity b_n is the function of n which descibes the shape of the light profile and it cannot be calculated analytically (Graham & Prieto, 1999; Khosroshahi et al., 2000; Möllenhoff & Heidt, 2001). It was evaluated as a root of an equation involving the incomplete gamma function (Wadadekar et al., 1999). The value was well approximated by $b_n = 0.87n - 0.14$. Sérsic function is represented in magnitude as,

$$\mu_b(R) = \mu_e + b_n \left[\left(\frac{R}{R_e}\right)^{\frac{1}{n}} - 1\right] \tag{1.3}$$

where, R_e is the effective radius of the bulge component, μ_e is the surface brightness at effective radius R_e, which is described as the radius of the circular aperature that contained half of the total light of the galaxy. n is the shape parameter otherwise called Sérsic index that controls the shape of the profile. If n is large, then the profile would be steeper with an extended wing. If the value of n is smaller, then a shallow inner profile would be produced with truncation at larger radius. b_n is the dependent variable coupled to Sérsic parameter n. A classic de Vaucouleurs profile defines the value of $n = 4$. The total flux is calculated either in integrated magnitude m_{tot} or in surface brightness magnitude μ_e. The equation of integrated magnitude is

$$m_{tot} = -2.5 \log\left(\frac{F_{tot}}{t_{exp}}\right) + zp \qquad (1.4)$$

where, m_{tot} is the total apparent magnitude and zp is the magnitude zeropoint. Zeropoint of an object is defined as the magnitude of an object that produces one count per second. The Sérsic profile with various n values is as shown in Figure 1.2. where R_e and μ_e are held fixed. It should be noted that larger the Sérsic index n, the steeper the central core, and more extended the outer wing. A low n has a flatter core and a more sharply truncated wing. Large Sérsic index components were very sensitive to uncertainties in the sky background level determination because of the extended wings (Peng et al., 2010).

1.5.2 Exponential disc profile

The exponential disk profile **defined by** Freeman (1970) is a special case of Sérsic function when $n = 1$ as shown in Figure 1.2. When $n = 1$, a relation exists between effective radius and disc scale length. i.e. $R_e = 1.678 R_d$, when $n = 1$. The exponential function is expressed as,

$$I_d(R) = I_d(0) \exp(-R/R_d) \qquad (1.5)$$
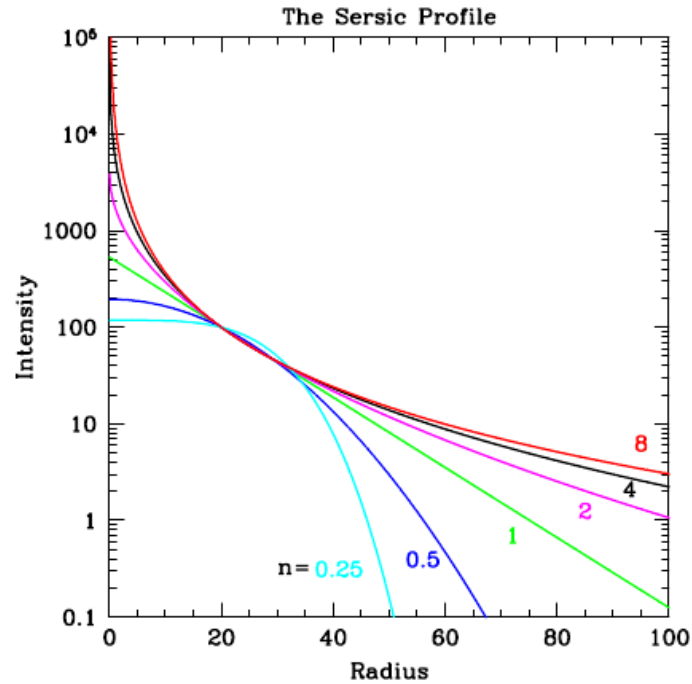
Figure 1.2: The Sérsic profile. Variation of larger and smaller value of n with radius defines the Sérsic and Exponential profile. Reprinted from Astronomical Journal, Chien Y.Peng © 2011, with permission from IOP Publishing for the American Astronomical Society (United States).

Where, $I_d(0)$ is the central disc intensity and R_d is the disc scale length. This equation represented in magnitudes as,

$$\mu_d(R) = \mu_d(0) + 2.5 \log_e(R/R_d) \tag{1.6}$$

where, $\mu_d(0) = -2.5 \log(I_0)$ is the disc central surface brightness.

1.6   Surface photometry-ellipse fit by IRAF

Since the galaxies are approximated by ellipses, fitting elliptical isophotes to the galaxies could be done (Davis et al., 1985). The ellipses are described fully by the center x_c , y_c, ellipticity, $\epsilon = 1 - b/a$, position angle θ and semi major axis a and

minor axis *b*. In an isophotal analysis the *ellipse* task reads two dimensional image section and fits a set of elliptical isophotes over an image. *Ellipse* is one of the tasks in *isophote* package provided by Space Telescope Science Data Analysis System (STSDAS)[1] /Image Reduction and Analysis Facility (IRAF)[2]. The result of the fitting could be written in STSDAS table that contain more than 40 columns. Each column contains the parameters of each isophote that are fitted to the galaxy. First isophote would be fitted with the guess values of center, ellipticity, position angle with predefined fixed semi-major axis length. At each step, the starting ellipse parameters would be taken from the previously fitted ellipse that had the closest semi-major axis length to the current one. With these values the image could be modelled along an elliptical path, to produce one dimensional intensity distribution as a function of position angle (Jedrzejewski, 1987). At the end of successful execution of the program, detailed output table would be produced which contains one row for each semi-major axis length. Each row contains the semi major axis length, mean isophotal intensity and its rms, ellipticity and its error, position angle and its error, minimum of valid data points in the fit, number of flagged data points extracted from the image, number of iteration and stop code. With the output table user can create the intensity profile, the variation of ellipticity, position angle with semi major axis. Errors in intensity, magnitude and local gradient can be obtained directly from the rms scatter of intensity data along the fitted ellipse. The isophotes of elliptical and S0 galaxies would not be a perfect ellipse. Quantifying the variation of intensity from being constant along the fitted ellipse is given by a Fourier series

$$I(\theta) = I_0 + \sum_{n=1}^{N}[a_n \sin(n\theta) + b_n \cos(n\theta)]$$

N is the highest order fitted ellipse, θ is the angle measured counter-clockwise from the major axis of the ellipse. where a_n , b_n are the harmonic amplitude related to the geometry of the ellipses which define the deviation of fitted ellipse from the true ellipse. The interactive mode of the analysis could be done with the help of

---

[1]http://ra.stsci.edu/STSDAS.html
[2]http://iraf.noao.edu

image server (Ximtool/SAOimage).

1.7   Photometry using GALFIT

GALFIT (Peng et al., 2002, 2010) is a two dimensional image analysis algorithm
written in C- language, that can model the light profiles of astronomical objects and
is a widely used tool to extract information about the astronomical objects (Peng
et al., 2010). Fitting a function to an image followed by analysis is very challenging
and in this context GALFIT proves to be advantageous in multi-component fitting
with an optimized computation speed along with user controlled analysis benefits.
Prior to program execution user could perform the preliminary analysis such as set-
ting the fitting region, identifying the position of the object and masking unwanted
neighbouring objects, extract the point spread function etc. GALFIT follows the
least square fitting method of non-linear type by a Levenberg-Marquardt algorithm
to find the optimum solution of the fit, which requires iterating to find best solu-
tion (Peng et al., 2010). GALFIT estimates the goodness of fit by determining χ^2
and computing the parameter adjustment for the subsequent step. The indicator of
goodness of fit is the normalized χ^2 or reduced χ^2_ν, described as

$$\chi^2_\nu = \frac{1}{N_{dof}} \sum_{x=1}^{nx} \sum_{y=1}^{ny} \frac{(f_{data}(x,y) - f_{model}(x,y))^2}{\sigma(x,y)^2}$$

Here N_{dof} is the number of degrees of freedom in the fit, nx and ny are the x and
y image dimensions; and $f_{data}(x,y)$ is the image flux at pixel (x,y). The $f_{model}(x,y)$
is the sum of m functions of f_ν (x, y; $\alpha 1$, . . . , αn), with n free parameters
($\alpha 1$, . . . , αn) in the 2D model. The uncertainty as a function of pixel
position, σ(x, y), is the Poisson error at each pixel, which can be provided as an
input image. If no σ image is given, one could be generated based on the gain and

read-noise parameters contained in the image header. Pixels in the image marked as being bad would not enter into the calculation of χ^2. Sky estimation would be done automatically, and user had an input option to find out the value of sky background (Peng et al., 2002).

1.7.1   Procedure of GALFIT

GALFIT works on several sequential steps: normalization and preparation of the input PSF image for convolution is the initial step, followed by cutting a section of image that contain the centre of the object to fit. Model image would be created based on the initial input parameters. For convolution, cutting the convolution region of model image created in the previous step would be done. By Fourier Transform Technique, convolution of the regions of model and derivative image with PSF image would be attained. The convolution region back into the model images would be then copied. Minimization would be done by comparison of the data image using Levenberg-Marquardt downhill-gradient method (Peng et al., 2002). Sequential processes from model image creation to minimization steps would be repeated until the required convergence is attained. Final output file and output images would be created in the last step.

1.7.2   Output files of GALFIT

After the completion of fitting process, GALFIT produces two text output files namely $fit.log$ and $galfit.NN$ and one output image block. $fit.log$ contains information about all the final parameters and error bars for the fit. The errors would be purely statistical. $galfit.NN$ contains all best fit parameters. NN specifies the number that keeps increasing so that it will never overwrite a previous fit. Output image block contains Image[1], Image[2] and Image[3]. The final fit parameters and a few input parameters are placed in the Flexible Image Transport System (FITS) header of image[2].

1.8 Scaling relations

Scaling relations are the relations between the physical properties of galaxies. It is useful to understand the formation processes of galaxies. The well known scaling relations used to study the early-type galaxies are the Kormendy relation (KR) and the Faber-Jackson relation (FJ). These two relations were considered as projections of the Fundamental Plane relation (FP), which is a three parameter relation. In the following subsections we discuss about these scaling relations.

1.8.1 Faber-Jackson Relation and Kormendy Relation

The relation between luminosity L and the stellar velocity dispersion σ of galaxies was first introduced by Faber & Jackson (1976) known as Faber-Jackson relation(FJ). Velocity dispersion is the term used for the measurement of kinematic motions of stars in pressure supported galaxies like ellipticals and in disc galaxies which are rotationally supported. The power law form of this relation is expressed as $L \propto \sigma^{\gamma}$. The value of γ varies from 3 to 5 and were reported in several studies (Bernardi et al., 2003; Reda et al., 2004; Desroches et al., 2007; La Barbera et al., 2010; Falcón-Barroso et al., 2011). The strong correlation between central surface brightness and effective radius of elliptical and bulges of lenticular galaxies was first suggested by Kormendy (1977) known as Kormendy Relation (KR). Djorgovski & Davis (1987) later modified this relation. Instead of central surface brightness they suggested mean surface brightness at effective radius as the good approximation, since it would be model independent and minimal effect of seeing. This relation is defined as,

$$<\mu_b(< R_e)> = a \log R_e + b \qquad (1.9)$$

where, $<\mu_b(< R_e)>$ is the effective surface brightness with in the half light radius. R_e is the half light radius defined as the radius of the central circular region that contains half of the total light of the galaxy. Slope of this relation a varies in the range of 2.0 to 3.0 (Kormendy, 1977).

1.8.2 Fundamental plane relation

Three parameter scaling relation that contains central velocity dispersion σ, effective radius R_e and mean surface brightness within R_e, ie, $<\mu_b(< R_e)>$ is called Fundamental plane relation(FP)(Djorgovski & Davis, 1987; Dressler et al., 1987). It reveals the dynamical properties of ETGs and the relation is expressed as

$$\log R_e = a \log \sigma + b<\mu_b(< R_e)> + c \tag{1.10}$$

where a and b are the coefficients of $\log\sigma$ and $<\mu_b(<R_e)>$ and c is the constant. σ is the value of velocity dispersion. Coefficients of a and b depends on the specific band for measuring the luminosity (Samir et al., 2016). If mass-to-light ratio was constant, then it reveals the homologus nature of early type galaxies and the plane is similar to virial plane. The coefficients satisfy a=2 and b=-1 defined by Faber & Jackson (1976) and the relation of the form of $R_e \propto \sigma^2 <\mu_e>^{-1}$. The deviation from this value in the observational analysis is called as the tilt of the FP. Jorgensen et al. (1996) obtained the FP coefficients $a = 1.24$ and $b = -0.82$ for local cluster early-type galaxies. Pahre et al. (1998) found that the coefficients for ellipticals observed in near-infrared are $a = 1.53$ and $b = -0.79$. The tilt of FP were studied by many authors, deviations of FP can be formed by variation of M/L ratio (Faber & Jackson, 1976), variations in stellar population in ETGs, sample from the field galaxies are some of the examples (Forbes et al., 1998; Reda et al., 2005).

1.9 Formation and evolution scenarios

The morphological analysis of galaxies are their correlation studies throw light regarding the formation and evolution scenarios of galaxies. Buta (2011) suggested that some unavoidable points such as the components present in galaxies, selection effect, the effect of environment, importance of multi wavelength analysis etc need to be considered while attempting to define the structure, formation and evolution of a galaxy. The two important components of galaxies are the central spheroidal bulge and the outer disc. The formation of these two components would be entirely

different, due to the difference in dynamical properties. Recent observational studies suggest the possibility of disc component in every galaxy including ellipticals (Emsellem et al., 2011; Naab & Burkert, 2001; Scorza & van den Bosch, 1998; Rix & White, 1990; Bender et al., 1989; Jorgensen & Franx, 1994; Bender et al., 1989). The existing formation scenarios of early-type galaxies are discussed below.

The two well known formation scenarios of galaxies are monolithic collapse model (Eggen et al., 1962; La Barbera et al., 2003; Kampakoglou et al., 2008; Tortora et al., 2013) and hierarchical formation model (Kauffmann, 1996; Kauffmann & Charlot, 1998). In monolithic collapse model, galaxies would be formed from early epoch at high redshift, from the collapse of a large single gas cloud (MacArthur et al., 2003). Stars would be formed in these case by a short (less than 1GYr) intense starburst. The galactic wind produced from this process that evacuates the extra gas present in the system, prevents later star formation. The final product of this process would be an elliptical galaxy dominated by population II stars. No further star formation would be possible because of the absence of cold gas.But in the hierarchical formation model, the concept depicts formation of galaxies by repeated processes of merging of smaller galaxies. Smaller halos would be formed initially and more massive ones be formed by the merging or from the accretion from the surrounding material (Boylan-Kolchin et al., 2006; Arp, 1966). This merging or accretion continues for larger structures like massive elliptical galaxies. This would be significant in cluster environment and possible in field also. In the monolithic concept, more massive systems like ellipticals would be formed first, but in hierarchical model less massive ones would be the starting point of galaxy formation. Figure 1.3 shows the two types of galaxy formation scenarios. The left side of the figure shows the monolithic collapse model and right side of the figure indicates the hierarchical model. From the study of light distribution of galaxies and the analysis of their structure, de Jong et al. (2004) found that the light distribution in elliptical galaxies were fitted by de Vaucouleurs $r^{\frac{1}{4}}$ law profile (de Vaucouleurs, 1948). The light profile of spiral galaxy disc were fitted with exponential profile defined by Freeman (1970) and bulge by de Vaucouleurs profile. From the generalization of Sérsic law described by Sérsic (1963) was possible to fit the central bright part of disc galaxy, independent of the inclination. From this it was identified that more than one type
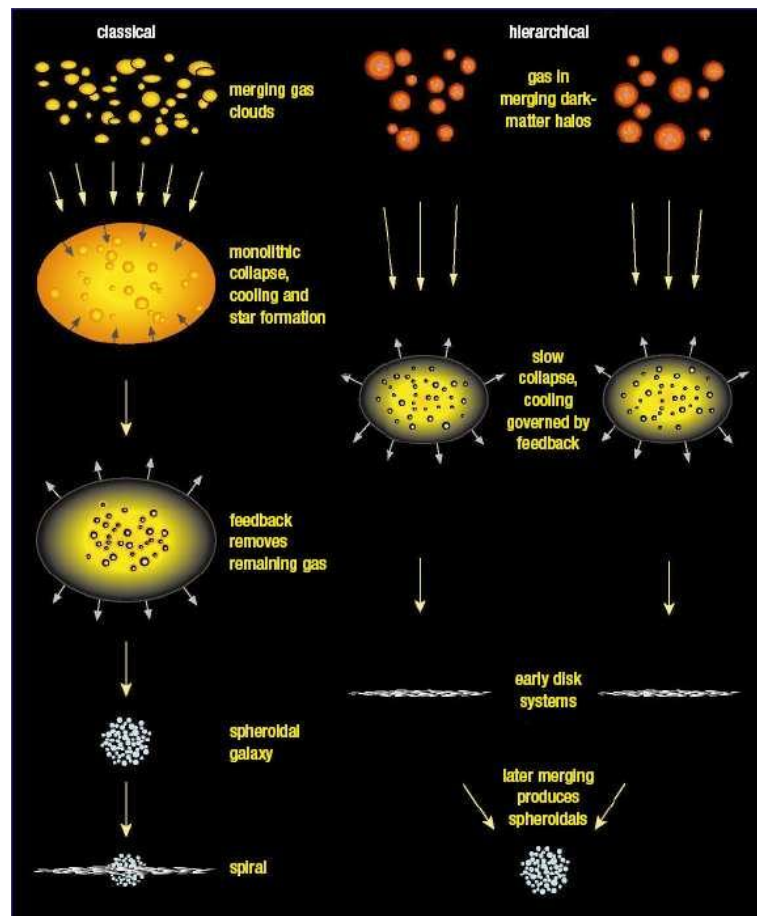
Figure 1.3: Two types of formation models. Left hand side shows the monolithic collapse model and right hand side shows the hierarchical model. Image Courtesy:http://jeffstanger.net/Astronomy

of objects with quite different physical properties and formation are situated at the galaxy centre. The shape of some bulges were different from ellipticals Athanassoula (2005) and had different kinematic properties. Athanassoula (2005) argued that different types of central components are present in a galaxy with properties similar to disc component. Based on their formation, bulges were classified mainly as three types: classical bulges, box /peanut bulges and pseudo bulges. The properties and formation of these three bulges were different; here we mention the main properties and the formation of classical and pseudo bulges.

1.10   components of galaxies and their properties

Elliptical galaxies are simple systems and considered as spheroidal in shape (ie, oblate or prolate shape by revolution). The disc galaxies containing an elliptical like bulge/ bar component and a disc component may display pronounced spiral structure (Binney & Merrifield, 1998). The three dimensional shape of bulges were analysed by the same technique applied for elliptical galaxies. But if the bulge present in a disc galaxy was more flattened towards the galactic plane, it would be difficult to disentangle the light from the disc. The bulges were formed in multiple ways. Psedo-bulges are different from classical bulges and formed through secular processes within a disc.

1.11   The classical bulges

Classical bulges are formed by gravitational collapse or hierarchical merging of smaller objects, and which were normally present in elliptical galaxies. Formation of these types of bulges could be from a short period of time, and it would be formed before the formation of a disc (Wyse et al., 1997). These bulges contained mainly older population and are ellipsoidal in shape. These have near-$r^{\frac{1}{4}}$ projected density profiles. The photometric radial profiles, their kinamatics mainly by the random motions of stars and their stellar populations are similar to that of elliptical galaxies (Athanassoula, 2005).

1.12   Disc like bulges or pseudo bulges

Another type of bulges was classified as disc like bulges or pseudo bulges, formed by the secular evolution processes in a galaxy (Kormendy & Kennicutt, 2004; Athanassoula, 2005; Genzel et al., 2008; Bournaud et al., 2014). Pseudo bulges exhibit a flattened structure and could be represented by an exponential luminosity profile. These bulges exhibited similar properties as that of a disc. It contains mainly young stellar population and rotates like a disc component and the kinematics of stars depend on their rotation (Athanassoula, 2005). These types of bulges are primarily found in late type systems as well as in early-type galaxies. Pseudo bulges may be

formed from the already existing discs formed either from monolithic collapse or from the hierarchical merging.

1.13   Nearby early-type galaxies in field

In this thesis we studied about early-type galaxies residing in a low density environment (Annibali et al., 2010). Early type galaxies represents ellipticals and S0 galaxies. The morphological classification of galaxies is clearly related to their environment (Dressler, 1980; Postman et al., 2005). Early type galaxies are seen mostly in clusters than in field and this was demonstrated by Dressler (1980) from the morphology density relation. From the homogenous properties and high luminosity, it was considered that most of the visible mass of the universe is related to early type galaxies (Renzini, 2006). The properties of early type galaxies depend on their environment see (Conselice et al., 2013). From the colour-magnitude relation (CMR) Dressler (1980) suggested that more luminous galaxies that are red in colour would be seen in denser regions. But the presence of morphological fine structures like ripples, shells and tidal tails could be usually seen in field galaxies (Malin & Carter, 1983; Zepf & Whitmore, 1993). From the scaling relations of FP (Dressler et al., 1987; Djorgovski & Davis, 1987)(see Section 1.) environmental dependence was studied in field, group and cluster by de Carvalho & Djorgovski (1992), and it was found that field galaxies have more scatter. The larger scatter was attributed to the extended star formation in the field early-type galaxies when the stellar population variables were included (Cappellari et al., 2006). Stellar population in early-type galaxies in different environments were studied by Reda et al. (2005) and it was suggested that field early type galaxies were more bluer, younger and more metal rich than cluster sample (Kuntschner et al., 2002; Terlevich & Forbes, 2002).

1.14   Outline of the thesis

We under took the morphological analysis of early-type galaxies in the nearby universe (z<0.02). Through the structural parameters obtained by the 2D decomposi-

tion analysis, we studied the different correlations between the parameters. These helped to gain better understanding regarding the formation and evolution of early type galaxies. The selected sample resides in low density environment. We used the images of galaxies were observed in near infrared K-band and spitzer 3.6 μm wavelength. K-band data for decomposition was easier and more better than the visible bands, as the absorption related problems were less in this band. So the smooth, featureless light profiles of galaxies in this band were very convenient for extraction of global disk and bulge parameters(Khosroshahi et al., 2000; Barway et al., 2009). The effect of sky extinction in IRAC 3.6μm was weaker than that of 2MASS K band (Gao et al., 2009). So we performed the decomposition analysis on the same sample observed in Spitzer 3.6μm also. Compared to the usual method of isophotal fitting, the bulge disc decompostion method provided better picture on the structure of galaxies, as it used complete information available on all pixels of the image.

In **Chapter 2** we discuss about the sample selected for the studies. Spectroscopically studied nearby early type galaxies that reside in the low density environment were selected. The images used were observed in 2MASS k-band and retrieved from IRSA. The 3.6μm images were oberved by Spitzer space telescope and retrieved from IRSA Spitzer. This chaper also discuss about the analysis technique IRAF and GALFIT used in our study.

Photometric analysis on near infrared images of the sample galaxies were described in **Chapter 3**. Preliminary analysis was done by the isophotal fitting using IRAF. Detailed analyses were done by two dimensional bulge disc decomposition method using GALFIT. The structural components of the galaxies were extracted by fitting the light profiles of bulge and disc using Sérsic and exponential functions. From this analysis we identified that the sample galaxies had significant disc component. We also studied the correlations of structural parameters and compared with the literature.

The photometric analysis of Spitzer observations were carried out in **Chapter 4**. The same procedure was repeated on these images also. From this analysis we identified that a clear distinction between the two types of bulges were present in

the sample according to the mean value of Sérsic index as 2.5. Lower value of Sérsic index ($n<2.5$) characterised pseudobulges and higher value of Sérsic index ($n>2.5$) characterised classical bulges. The pseudo bulges and classical bulges present in our sample showed different relations of the structural parameters. From the correlation of structural studies we identified a strong correlation (r=0.95) between the bulge effective radius and disc scale length for pseudobulges than classical bulge galaxies. This relation suggested that the formation of bulges in these galaxies were from already existing disc by secular evolution.

Chapter 5 summarise the thesis with our main findings of 2MASS and Spitzer image analysis. We had also mentioned the scope of future research in the field of photometric structural studies.

Chapter 2

Sample, Observations and Data Reduction

2.1 Introduction

In this chapter we discuss about the sample and its properties. The main objective of the study focus to gather the structural information about the early-type galaxies through observations in infrared, so as to understand the formation and evolution scenarios of such galaxies. Early-type galaxies reside in cluster and in field also. We chose low density region sample for photometric studies. Dust extinction would be significantly less in near infrared images and hence can provide more details on structure than optical images (Väisänen et al., 2002). Owing to the shallowness of near infrared images from Two Micron All Sky Survey (2MASS), additional analysis by Spitzer images in the deeper observations were performed to augment the 2MASS findings. We selected the near infrared images in two wave bands of K_s and J, at wavelength of 2.16 μm and 1.25 μm from 2MASS archive. The mid-infrared images from the Spitzer Science Survey with the wavelength of 3.6 μm was used.The Spitzer image studies were carried out as continuation of the 2MASS findings. The preliminary structural analysis was carried out by the *ellipse* task in $IRAF$ and the structural parameters used in the analysis were extracted by the two dimensional bulge-disc decomposition method, GALFIT.

2.2   Sample

Spectroscopic data of 65 early-type galaxies which contain 45 ellipticals and 20 lenticulars were studied and reported by Annibali et al. (2007, 2010). We had selected this sample for photometric structural analysis. The main properties of this selected sample of galaxies were that all of them contained ionised gas (Roberts et al., 1991) and most of them exhibited morphological fine structures and dust content. Out of 65 galaxies, we chose 54 galaxies with 37 ellipticals and 17 lenticulars for 2MASS image analysis. Others with no observational images are available in 2MASS survey. Out of these 54 galaxies we used 39 galaxies that consists of 26 ellipticals and 13 lenticulars for Spitzer image analysis. No Spitzer images were observed for others. The morphological classification of the sample was purely based on the Third Reference Catalogue (RC3) (de Vaucouleurs, 1991). All galaxies were present in the Revised Shapely-Ames Catalog of Bright Galaxies (RSA) (Sandage & Tammann, 1987). As per the available literature, 70% of the sample galaxies were fast rotators and 30% were slow rotators (Emsellem et al., 2011). Early-type galaxies were commonly seen in cluster environment (Dressler, 1980) with older stellar populations. Our sample galaxies which contain ionised gas, mainly reside in low density environment. In the forthcoming chapters we discuss about the photometric scaling relations as well as the correlation between different structural parameters and global photometric properties. The selected sample exhibits the following properties

- Redshift of the sample <0.02, taken from Nasa Extra galactic Database (NED)[3].

- Values of velocity dispersion were adopted from Lyon Meudon Extragalactic Database, HYPERLEDA[4] that varied from 115 to 340 $\mathrm{km\,s^{-1}}$.

- The local density of galaxies varied from $\sim 0.1 \mathrm{Mpc^{-3}}$ for isolated galaxies and $4 \mathrm{Mpc^{-3}}$ for galaxies in the region of Virgo cluster. The definition of cluster based on Tully catalogue (Tully, 1988) for Fornax cluster members like NGC1399 and NGC1389 had density 1.59 and $1.50 \mathrm{Mpc^{-3}}$.

---

[3]https://ned.ipac.caltech.edu/
[4]http://leda.univ-lyon1.fr

Galaxy Name	R. A. (J2000)	Dec. (J2000)	Distance (Mpc)	Type (RSA)	(RC3)	σ_c km s^{-1}
NGC 0128	00 29 15.0	+02 51 51	53.9	S0₂(8) pec	S0 pec sp	183
NGC 0777	02 00 14.9	+31 25 46	66.0	E1	E1	317
NGC 1052	02 41 04.8	-08 15 21	17.8	E3/S0	E4	215
NGC 1209	03 06 03.0	-15 36 41	33.5	E6	E6	240
NGC 1366	03 33 53.7	-31 11 39	15.4	E7/S0₁(7)	S0 sp	120
NGC 1380	03 36 27.6	-34 58 34	24.5	S0₃(7)/Sa	SA0	240
NGC 1389	03 37 11.8	-35 44 44	11.4	S0₁(5)/SB0₁	SAB(s)0-	139
NGC 1407	03 40 11.8	-18 34 48	22.8	E0/S0₁(0)	E0	286
NGC 1426	03 42 49.1	-22 06 30	18.3	E4	E4	162
NGC 1521	04 08 18.9	-21 03 07	57.7	E3	E3	235
NGC 1533	04 09 51.8	-56 07 06	10.6	SB0₂(2)/SBa	SB0-	174
NGC 1553	04 16 10.5	-55 46 49	14.7	S0₁/2(5)pec	SA(r)0	180
NGC 1947	05 26 47.6	-63 45 36	15.8	S0₃(0)pec	S0-pec	142
NGC 2749	09 05 21.3	+18 18 47	62.0	E3	E3	248
NGC 2962	09 40 53.9	+05 09 57	31.7	RSB0₂/Sa	RSAB(rs)0+	−
NGC 3136	10 05 48.1	-67 22 41	26.0	E4	E:	230
NGC 3268	10 30 00.6	-35 19 32	43.1	E2	E2	227
NGC 3489	11 00 18.6	+13 54 04	14.1	S0₃/Sa	SAB(rs)+	129
NGC 3557	11 09 57.6	-37 32 21	47.1	E3	E3	265
NGC 3607	11 16 54.6	+18 03 06	17.6	S0₃(3)	SA(s)0:	220
NGC 3818	11 41 57.3	-06 09 20	28.5	E5	E5	191
NGC 3962	11 54 40.1	-13 58 30	30.0	E1	E1	225
NGC 4374	12 25 03.7	+12 53 13	18.5	E1	E1	282
NGC 4552	12 35 39.8	+12 33 23	9.14	S0₁(0)	E	264
NGC 4636	12 42 49.8	+02 41 16	17.5	E0/S0₁(6)	E0-1	209

Table - continued.

Galaxy Name	R. A. (J2000)	Dec. (J2000)	Distance (Mpc)	Type (RSA)	(RC3)	σ_c km s^{-1}
NGC 4696	12 48 49.2	-41 18 39	44.8	E3	E+1 pec	254
NGC 4697	12 48 35.9	-05 48 03	21.7	E6	E6	174
NGC 5011	13 12 51.8	-43 05 46	47.3	E2	E1-2	249
NGC 5044	13 15 24.0	-16 23 08	42.8	E0	E0	239
NGC 5077	13 19 31.7	-12 39 25	43.1	S01/2(4)	E3+	260
NGC 5090	13 21 12.8	-43 42 16	50.9	E2	E2	269
NGC 5193	13 31 53.5	-33 14 03	52.2	S01(0)	E pec	209
NGC 5266	13 43 02.1	-48 10 10	44.6	S03(5) pec	SA0-:	199
NGC 5328	13 52 53.3	-28 29 22	69.5	E4	E1	303
NGC 5363	13 56 07.2	+05 15 17	19.4	S03(5)	I0	199
NGC 5638	14 29 40.4	+03 14 00	26.3	E1	E1	168
NGC 5812	15 00 55.7	-07 27 26	29.9	E0	E0	200
NGC 5831	15 04 07.0	+01 13 12	25.5	E4	E3	164
NGC 5846	15 06 29.3	+01 36 20	26.2	S01(0)	E0+	250
NGC 5898	15 18 13.5	-24 05 53	31.7	S02/3(0)	E0	220
NGC 6721	19 00 50.8	-57 45 34	60.5	E1	E+	262
NGC 6758	19 13 52.3	-56 18 36	46.1	E2(merger)	E+:	242
NGC 6776	19 25 19.1	-63 51 37	75.5	E1 pec	E+pec	242
NGC 6868	20 09 54.1	-48 22 46	37.5	E3/S02/3(3)	E2	277
NGC 6875	20 13 12.5	-46 09 42	41.0	S0a(merger)	SAB(s)=pec:	–
NGC 6958	20 48 42.6	-37 59 51	34.6	R?S01(3)	E+	223
NGC 7097	21 40 12.9	-42 32 22	33.0	E4	E5	224
NGC 7135	21 49 46.0	-34 52 35	32.9	S01 pec	SA0-pec	231
NGC 7332	22 37 24.5	+23 47 54	11.6	S02/3(8)	S0pec sp	136
NGC 7377	22 47 47.5	-22 18 44	41.7	S02/3/Sa pec	SA(s)0+	145
IC 1459	22 57 10.6	-36 27 44	21.1	E4	E	311
IC 2006	03 54 28.4	-35 58 02	18.0	E1	E	122
IC 3370	12 27 37.3	-39 20 16	44.6	E2 pec	E2+	202
IC 5063	20 52 02.3	-57 04 08	45.3	S03(3)PEC/Sa	SA(s)0+:	160

Table 2.1: Properties of the sample. (1) Host galaxy name; (2) Right Ascension in hours, minutes and seconds; (3) Declination in degrees, arc minutes and arc seconds; (4) Distance in Mpc from NED; (5) and (6) Morphological type from RSA and RC3 respectively, (7) Velocity dispersion from HYPERLEDA.

2.3   Observations

2.3.1   The Two Micron All Sky Survey (2MASS)

Near infrared astronomy is one among the main branches of astronomy and astrophysics that used the observation at the wavelength from 0.75 to 300 μm. 2MASS project covers 99.998% of the sky with milli Jansky sensitivity and arcsecond resolution in NIR wavelength (Skrutskie et al., 2006). It was a ground based observation that scaned the whole sky in the three near-infrared bands such as J (1.25 μm), H (1.65 μm) and K_s(2.16 μm). The selected pixel scale was of $2'' \times 2''$ with 7.8 seconds of integration time for each sky observation. It used two highly-automated 1.3-m telescopes, among which one was situated at Mt.Hopkins, Arizona ($N31°\ 40'50''.8$, $W110°\ 52'41''$), and other at Cerro Tololo, Chile ($S30°\ 10'3''.7$, $W70°\ 48'18''$). Each of the telescopes contained three Near Infrared Camera and Multi Object Spectrometer (NICMOS3) 256×256 HgCdTe arrays with 40μm pixel pitch and were sensitive between wavelengths of 0.8 and 2.5 μm. Each camera contained two dichroic mirrors which help the simultaneous imaging of an $8'.5 \times 8'.5$ field at a pixel scale of $2''\ pixel^{-1}$ in the three wavebands (Skrutskie et al., 2006). The preprocessing was already done by an automated software pipeline of 2MASS project and it provided calibrated images. The final database from the 2MASS observation contained a Point Source Catalogue and an Extended Source Catalogue along with FITS image in 2MASS All-Sky Data Release[5] The mosaic images we used were obtained from IRSA-2MASS[4]. This mosaic images can be obtained only for registered users. As per our selection criteria they provided the final data set. Data set includes the FITS and jpeg images. .

The major scientific benifits of 2MASS observations are listed as below

- Free to observe the objects with the lesser effect of interstellar dust and gas (Barway et al., 2009).

- Dominated the older and redder stellar populations (Jarrett et al., 2000).

---

[5]http://www.ipac.caltech.edu/2mass/releases/allsky/
[4]http://hachi.ipac.caltech.edu:8080/montage/

2.3.2   Spitzer observations

Spitzer space telescope was one of the space missions of NASA that started in August 2003. Spitzer telescope contained 3 main instruments namely Infra Red Array Camera (IRAC), Infra Red Spectrograph (IRS) and Multiband Imaging Photometer for Spitzer (MIPS). IRAC is a four channel camera that provides images of $5.2' \times 5.2'$ at 3.6, 4.5, 5.8 and 8.0 microns. Two adjacent fields of view were imaged in pairs (3.6μm and 5.8μm; 4.5μm and 8.0μm) by dichroic beam splitters. All the four detector arrays in the camera were 256×256 pixels in size, with a pixel size of $1.2'' \times 1.2''$. The two detectors in the shorter wavelength bands 3.6μm and 4.5μm of IRAC (Fazio et al., 2004) could be treated as stellar mass tracers of nearby galaxies. The two instruments that constitute the IRS performs low and high resolution spectroscopy. The MIPS provides for both imaging and photometry. This was carried out in broad spectral bands centered nominally at 24, 70, and 160μm, and for low resolution spectroscopy between 55 and 95 μm. The Spitzer Science Center (SSC) conducted the science operations for Spitzer. After the completion of the observation procedure the resulting data which are pipeline processed were placed in Spitzer Heritage Archive (SHA).

2.3.3   2MASS Images

2MASS images were downloaded from IRSA website. Images of each galaxy were available in three different wavelengths of J(1.24μm), H(1.66μm) and K$_s$(2.16μm) bands and we chose the J and K band images for analysis. The sky value was measured and subtracted from the image frame and accordingly the sky subtracted images were used for the analysis. The point sources and unwanted pixels present in the image frame were masked successfully so as to eliminate its effect on the luminosity of the target galaxy.

2.3.4   Spitzer Images

Spitzer images were obtained from the Spitzer Heritage Archive (SHA) website hosted by the Infrared Science Archive IRSA. Each individual observation was identified by Astronomical Observation Request (AOR). Each AOR key had an option to select the type of data. Level 1 Basic Calibrated Data (BCD) file was selected for our analysis. The unprocessed raw data were available in level 0. BCD files contained four sets of data, according to the observation of four channels based on four wavelengths 3.6, 4.5, 5.6 and 8 μm. We selected the channel 1 of 3.6 μm wavelength data file. Each data file contained different types of image files, which included basic calibrated image files, associated uncertainty image files and bad pixel mask files. All these images were in the $fits$ format and details of these images were available in their header. The details about the Spitzer observations and the instruments were available in the Spitzer instrument handbook[6].

2.3.5   MOPEX

The Spitzer Science Center (SSC) developed the astronomical software package 'MOPEX', mainly used for convertion of the downloaded images into science grade images. MOPEX contains a set of pearl scripts and runs a number of individual modules written in C/C++ language. It processes the calibrated data obtained from spitzer SHA website and works on command line or in Graphical User Interface (GUI). We selected the user friendly GUI mode.The basic processing steps include combining a stack of input images into mosaic and doing point-source photometry. After the input data file was obtained, the unified co-ordinate system would be generated. Subsequently the background matching process would begin. Levelling the background of input image by overlapping was the main operation carried out by MOPEX. It corrects the variation in the background level of each frame by addition of a constant value. The next step was the image interpolation processes that projects the input images and interpolates the images onto the unified code and further the input pixel values would be given to the output array. Another main feature of the MOPEX could be pointed out as the outlier detection and rejection.

---

[6]http://irsa.ipac.caltech.edu/data/SPITZER/docs

Cosmic rays would be determined and rejected accurately by applying more than one outlier detection. Image co-addition task of MOPEX provides clean mosaic image with no cosmic rays. This image, considered as the science grade image was sky subtracted and was used for our analysis. The BCD file contained number of mosaic images (maic.fits), uncertainty maps (bunc.fits) and bad pixel masks (bimask.fits). MOPEX mosaiced each of these images and produced a single mosaic image, uncertainty image and mask image. The zero point magnitude used for Spitzer image of 3.6 μm observation was 20.022.

The photometric analysis of early-type galaxies in the infrared observations is presented in this section. The analysis was carried out using IRAF and GALFIT.

2.4 Photometric analysis using IRAF

Sample containing 54 early-type galaxies obtained from 2MASS and 39 galaxies from Spitzer were analysed. The details of sample galaxies were described in Section 2.2. The analysis was done by fitting the elliptical isophotes on each of the galaxies using IRAF/STSDAS.

2.4.1 Isophotal fitting

IRAF/STSDAS was used for fitting the smooth elliptical isophote on the images. We started fitting from smaller radius of 10 arcsec to the higher value as per the size of the galaxy. The center of the galaxy was identified by the use of *imcntr* command from IRAF. The ellipticity and position angle were obtained from RC3. These values were given to IRAF as the initial guess values and set to vary at the time of fitting. After the successful completion of the isophotal fitting, the output table was produced which contained the isophotal information about each of the galaxies. The tasks listed below were used for the analysis of isophotal fitting.

- *ellipse* for fitting the elliptical isophote over an image

- *isoplot* for plotting the isophotal parameter against semi major axis

- *isopall* for plotting all the nine isophotal parameters against semi major axis

- *isomap* for drawing the contour map over the image

From this ellipse fitting, we got the surface brightness profile, variation of ellipticity and position angle against semi major axis. The fourth order fourier component from the output was useful to study the deviation of isophote from a perfect ellipse. A positive value ($b_4 > 0$) suggested an excess of light in the major or minor axis, which defines a discy isophote while a negative value ($b_4 < 0$) suggested a boxy isophote. The details about surface photometry by ellipsefit method was provided in Section 1.6.

2.4.2   Residual Images

Another method to analyse the structure was the study of the residual image. The residual images were created by subtracting the model of the galaxy created by isophotal fitting from the original image. The *bmodel* task in IRAF was used for creating the 2D model of the galaxy, which represented the smooth elliptical structure of the galaxy. This model was created with the help of the output from isophotal fitting. The model subtracts only the smooth galaxy profiles from the image and any additional components or hidden components present in the galaxy (eg: dust, shells, discy, boxy) would be shown in the residual image.

2.5   Photometric analysis using GALFIT

One dimensional and two dimensional methods of surface photometric analysis were described in Section 1.3, and it could be pointed out that the single component fitting and 1D fitting were not the only method used to understand the structure of a galaxy. The detailed structural analysis of our sample galaxies were done by two dimensional bulge disc decomposition method. The algorithm GALFIT was used for modelling the different components of galaxies. The details about the GALFIT were provided in Section 1.7. Analysis was started by using the 2MASS images. The input template file of GALFIT for fitting the images is shown in Figure 2.1.

```
============================================================
==================
# IMAGE and GALFIT CONTROL PARAMETERS
A) Input image .fits          #Input data image (FITS fi1407_k_mosaic.fitsle)
B) Output image.fits          #Output data image block
C) None                 #Sigma image name (made from data if blank or"none")
D) None                 #Input PSF image and (optional) diffusion kernel
E) 1                    # PSF fine sampling factor relative to data
F) Bad pixel mask.fits        # Bad pixel mask (FITS image or ASCII coord list)
G) none                      # File with parameter constraints (ASCII file)
H) xmin xmax ymin ymax  #Image region to fit (xmin xmax ymin ymax)
I) **   **                   # Size of the convolution box (x y)
J) 20.2020                    # Magnitude photometric zeropoint
K) 1.0  1.0                    # Plate scale (dx dy)   [arcsec per pixel]
O) regular              # Display type (regular, curses, both)
P) 0                    # Options: 0=normal run; 1,2=make model/imgblock & quit
# INITIAL FITTING PARAMETERS
# Sersic function
0) sersic               # Object type
1) x_centre  y_centre 1 1    # position x, y      [pixel]
3) 8.0            1      # total magnitude
4) 10.0           1      #   R_e           [Pixels]
5) 4.0            1      # Sersic exponent (deVauc=4, expdisk=1)
9) 0.95           1      # axis ratio (b/a)
10) 0.0           1      # position angle (PA)  [Degrees: Up=0, Left=90]
Z) 0                    #  Skip this model in output image?  (yes=1, no=0)


# Component number: 2
0) expdisk                  #  Component type
1) x_centre  y_centre 1 1   #  Position x, y
3) 7.0            1      #  Integrated magnitude
4) 20.0           1      #  R_s (disk scale-length)   [pix]
9) 0.95           1      #  Axis ratio (b/a)
10) 0.0           1      #  Position angle (PA) [deg: Up=0, Left=90]
Z) 0                    #  Skip this model in output image?  (yes=1, no=0)
# sky
0) sky
1) 0.0            0      # sky background      [ADU counts]
2) 0.000          0      # dsky/dx (sky gradient in x)
3) 0.000          0      # dsky/dy (sky gradient in y)
Z) 0                    #  Skip this model in output image?  (yes=1, no=0)
```

Figure 2.1: Input template file of GALFIT; First component prefferd for Sérsic function and second component prefered for exponential function

Original image and mask images were provided in 'fits' format. The center and zero point magnitude were given as the same as we used for isophotal fitting. The ellipticity, position angle and total magnitude were considered as the initial guess values obtained from the isophotal fitting. In the first trial of the analysis, only the single Sérsic component was used for fitting. In the analysis, the sky was used as one of the components for the fitting. From the second trial onwards the obtained sky value from the first trial was fixed. Because the sky values in near infra-red are usually very high. Hence it becomes difficult for the code to identify the disc (and bulge) parameters accurately, as the associated Poisson noise in the sky background also will be large. Hence it is advised to fix the background while running the code to extract structural parameters (Ravikumar et al., 2006). After successful completion of the fitting of galaxies by single Sérsic component, we attempted to find out the disc component in the nearby early-type galaxies including ellipticals. Accordingly each of the sample galaxies was modelled by exponential and Sérsic functions. The components of bulge and disc and the measured values after the fitting of each galaxy were given in Chapter 3 and Chapter 4. Already present disc components of the lenticular galaxies were quantitatively measured by the two dimensional algorithm. As the 2MASS images were shallow, we could not reliably establish the existence of large and strong discs in elliptical galaxies. Hence we considered the Spitzer observation which is deeper than the 2MASS.

The science grade Spitzer images that we created with the help of MOPEX were used for the bulge disc decomposition analysis. These images were already sky subtracted. The input file of GALFIT needs additional images os PSF image, bad pixel mask image, sigma images etc. The mask images were created with the help of modified Source Extractor (Bertin & Arnouts, 1996) file. The Spitzer IRAC data with the pixel resolution as 1.2 arcsec, was very close to the Gaussian function of point sources (Peng et al., 2010). The IRAC PSF had wide wings, and was dependent on the instrument orientation (Salo et al., 2015). So the large convolusion box sizes were needed for decomposition. The seperate PSF image were created by the function Gaussian by GALFIT. The parameters of Gaussian, were determined from the brightest stars detected by Source Extractor (Bertin & Arnouts, 1996) present in each image. Sigma images were created by MOPEX by the estimation of the noise from each BCD data. Spitzer archive that already provided the uncertainty

images for each of the BCD data and were co-added and produced single output by the task of S/N estimator present in the overlap module in MOPEX software package. First trial of our analysis on Spitzer images was done for single Sérsic fit and then the exponential function to model the disc components was added.

In the next chapter we discuss the photometric structural analysis on the NIR images obtained from 2MASS.

Chapter 3

Photometric analysis of early-type galaxies in near infrared using 2MASS images

3.1 Introduction

In the previous chapter, we described 54 early-type galaxies observed in near infrared. The photometric structural analysis of sample galaxies in J and K bands is presented through this chapter. With the J and K band images, the photometric parameters such as luminosity, effective radius, surface brightness and magnitude of sample galaxies were measured by the surface brightness profile analysis. The possibilities of additional components present in the galaxies were also studied by detailed two dimensional image analysis. With the obtained information, we tried to explore the possible formation scenarios of these systems through correlation analysis.

3.2 Analysis and Results

Isophotal fitting is a common and simple method to perform surface photometry. Our work was initiated by fitting of elliptical isophotes on the images and were done by the *ellipse* task in IRAF/stsdas. The radial profiles were subsequently studied. The fourth order Fourier components in the fitting mentioned in previous chapters
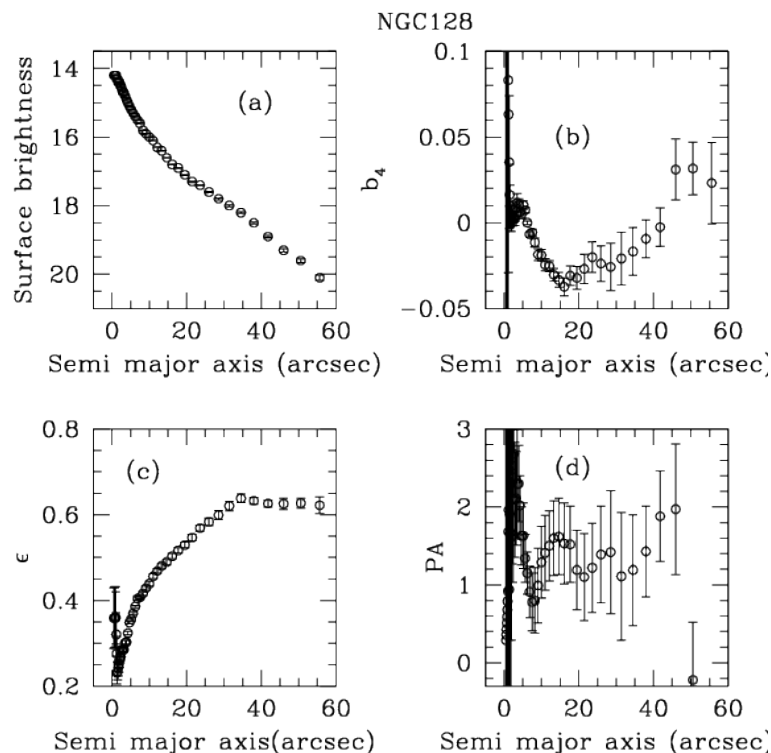
Figure 3.1: Structural parameters obtained from ellipsefit and their properties : Variation of Surface brightness(a), b_4 component(b), ellipticity(c) and position angle(d) along semi major axis.

(see Section 1.6 and Section 2.4) were used to recognize the deviation from perfect ellipses (Bender & Moellenhoff, 1987). Any additional amount of light present in a galaxy shows up as a deviation from a perfect ellipse. The excess light along the major and minor axis of the galaxy would be indicated by a positive or a negative value of b_4. Positive values of b_4 suggest a discy isophote and negative values indicate boxy isophotes. Some of the examples of the isophotal analysis are shown in Figure 3.1 and Figure 3.2.

An example for a boxy isophote present in our sample is shown in Figure 3.1. The variation of magnitude, ellipticity, position angle and b_4 components are also shown in this figure. Most of the points represented negative value of b_4 which indicated that this galaxy had a boxy isophote. It was studied and reported by D'Onofrio et al. (1999) through photometric studies in optical and NIR that, this galaxy contains boxy or peanut shaped bulge. An X-like feature was identified by
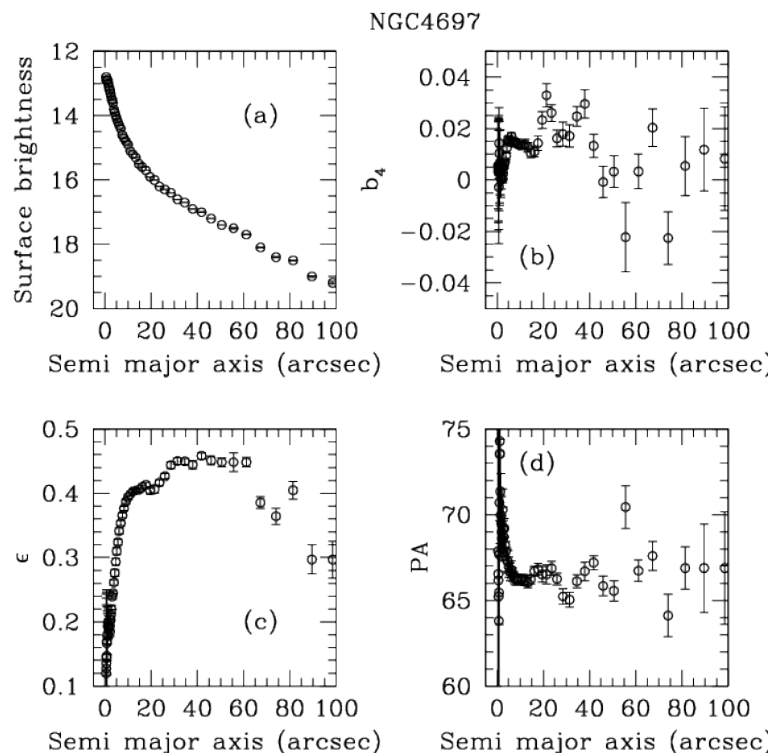
Figure 3.2: Structural parameters obtained from ellipsefit and their properties : Variation of Surface brightness(a), b_4 component(b), ellipticity(c) and position angle(d) along semi major axis.

Combes et al. (1990) and Emsellem & Arsenault (1997) in the center of this galaxy. They also suggested that the bulge present in the galaxy as boxy/peanut shaped bulge. From profile analysis, we could not identify the X-like feature, but in residual image we obtained the feature at the center as shown in Figure 3.3.

In Figure 3.2 variations of surface brghtness, b_4 component, ellipticity and position angle are shown for the galaxy NGC4697. As the values of b_4 remains mostly positive, the ellipse fit suggests the presence of a discy galaxy. Further, both ellipticity and position angle profiles show a sudden variation around $20''$, indicating the possibility of existance of additional component(s) to the smooth bulge component. Near the centre of the galaxy image, the effect of psf is maximum and isophotes tend to be nearly circular. Hence the variations found in position angle, ellipticity and b_4 component near the centre need not to be treated seriously. At the outskirts of the galaxy on the other hand the parameters show high errors associated in these

measurments, possibly due to the background sky intensity.

The ellipsefit method was already discussed in Chapter 2. It is considered as a partial 2D fitting method as it uses intensity details selectively (along the ellipse only) from the image. GALFIT on the otherhand, is a full 2D method that use data from all available pixels. The decomposition by GALFIT is discussed in next section.

3.3   Surface Photometry using GALFIT

3.3.1   Two dimensional bulge disc decomposition

Each of the sample galaxies in J and K bands from 2MASS observation was modeled using Sérsic and exponential functions. By this method, we got magnitude, size, ellipticity and position angle and accordingly estimated the absolute magnitude, colour and surface brightness for both bulge and disc components of the galaxy. Table 3.1 shows data obtained from the GALFIT, and Table 3.2 includes data that are estimated by the formula (See Section 3.3.2). In the first trial we fitted the projected surface brightness profile of each of these galaxies assuming a single Sérsic profile. Secondly, all the galaxies were fitted for a bulge and disc component with assumption of Sérsic and exponential profiles respectively.

Figure 3.3 represents an edge on galaxy NGC128 mentioned in isophotal fitting. Compared to isophotal fitting, 2D decomposition was found to be better to trace the components correctly with use of every pixel of an image. Compared to single Sérsic model Sérsic and exponential model had better χ^2 value. Similarly Figure 3.4 depicts an elliptical galaxy NGC4374 which we modeled by isophotal fitting, single Sérsic as well as by Sérsic and exponential functions. Two component model have better χ^2 value.

3.3.2   Photometric parameters measurement

The total light of a galaxy comes from the combined contributions of the various components present in the system. Our sample was modeled by a bulge and a disc component and hence the total light measured was a combination of Sérsic and
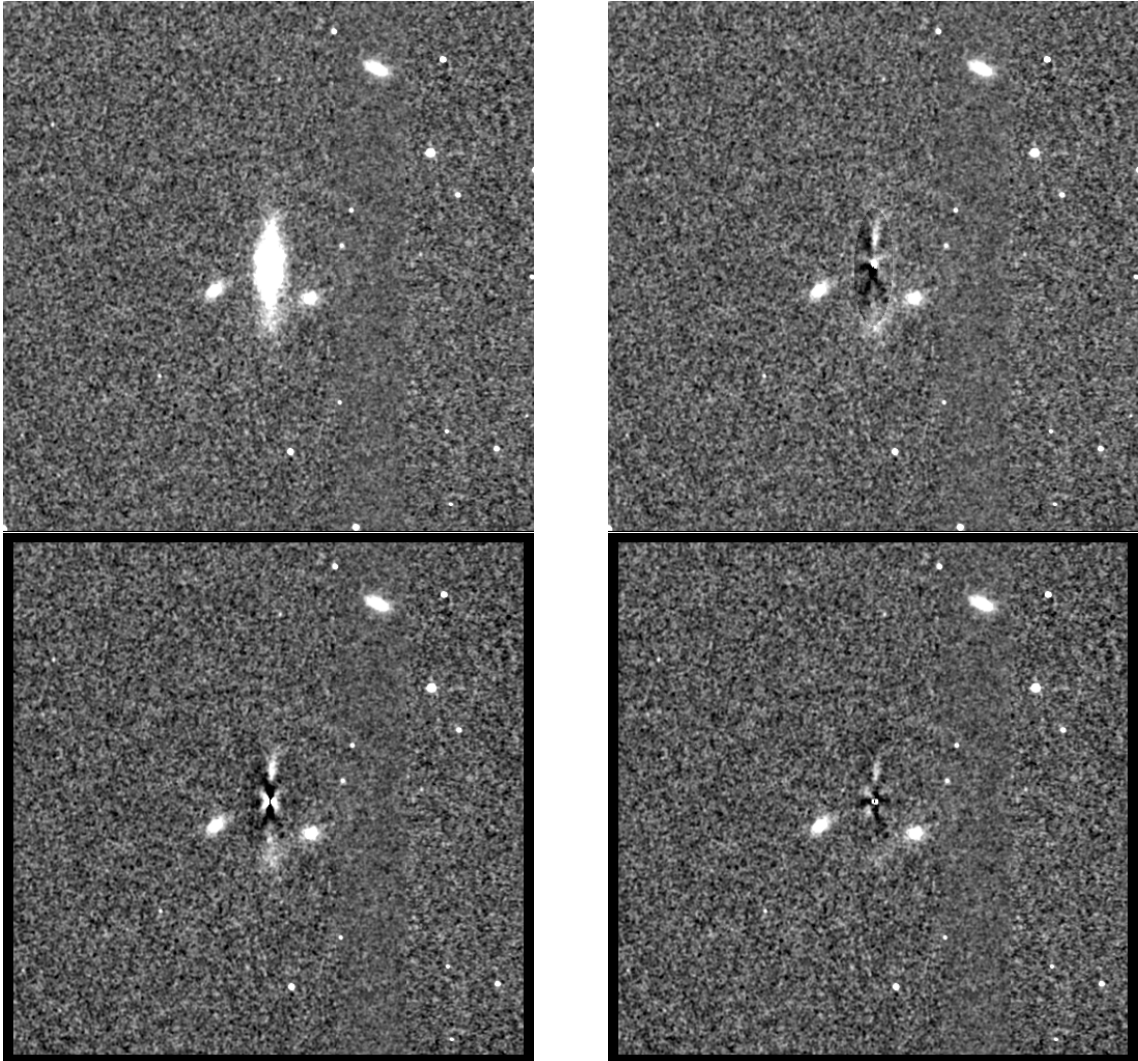
Figure 3.3: Original image and residual images of NGC128: Original image obtained from 2MASS observation (top left), residual image obtained by ellipse model subtracted from the original image by isophotal analysis (top right), residual image obtained by Sérsic model subtracted from the original (bottom left) and residual image obtained by Sérsic and exponential component model subtracted from the original image (bottom right).
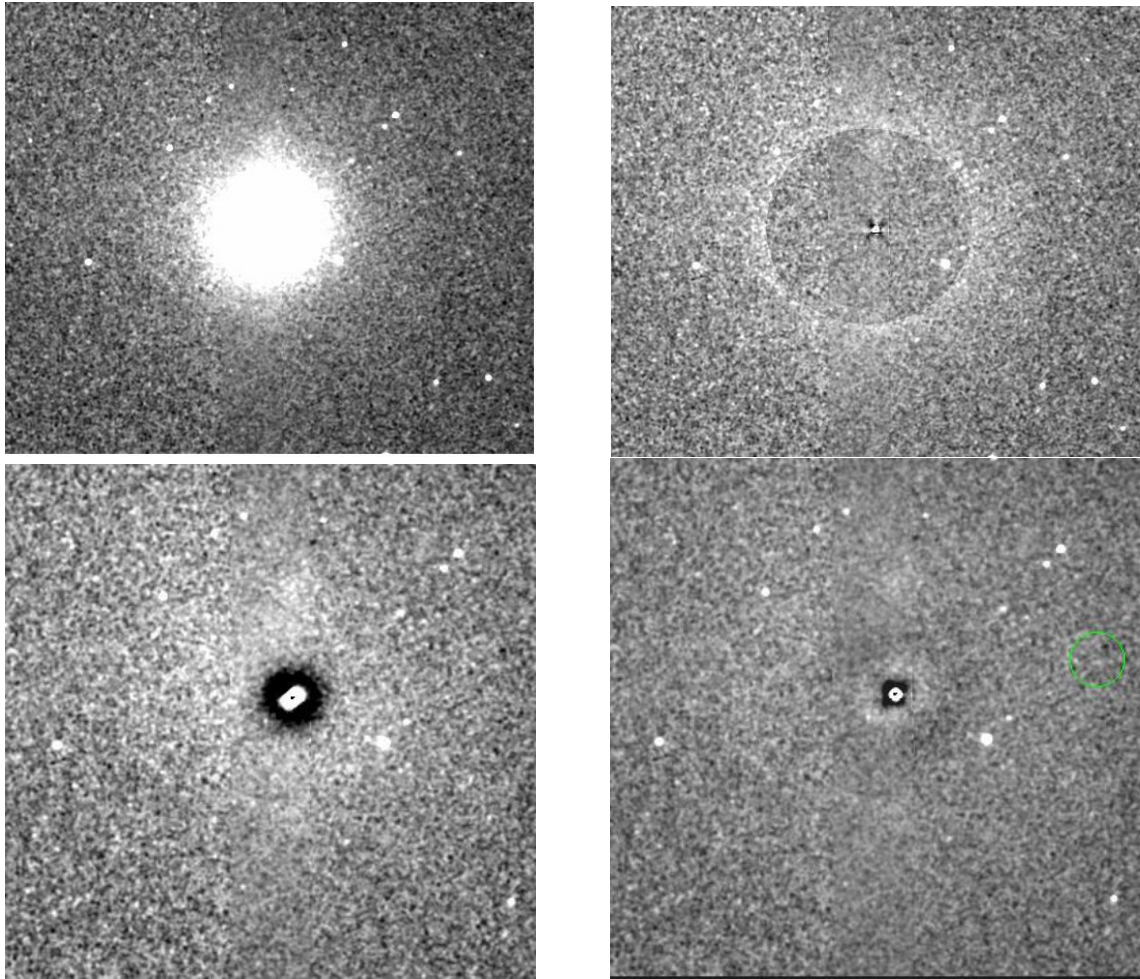
Figure 3.4: Original image and residual images of NGC4374: Original image obtained from 2MASS observation (top left), residual image obtained by ellipse model subtracted from the original image by isophotal analysis (top right), residual image obtained by Sérsic model subtracted from the original using GALFIT (bottom left) and residual image obtained by Sérsic and exponential component model subtracted from the original image using GALFIT (bottom right).

exponential functions described as,

$$I_{tot} = I_{bulge} + I_{disc} + I_{sky} \qquad (3.1)$$

where, I_{bulge} is the projected bulge intensity distribution described by Sérsic power law, I_{disc} is the contribution of light from the disc component expressed by an exponential function and I_{sky} is the intensity of sky background. The surface brightness of sample galaxies was also measured. The average surface brightness was measured using the equation,

$$<\mu_b(< R_e)> = m + 2.5\log(2\pi R_e^2) \qquad (3.2)$$

where, m is the apparent magnitude of the galaxy, R_e is the effective radius in arcsec and $<\mu_b(< R_e)>$ is mean surface brightness within effective radius. The other calculated parameters were colour (J-K), which is defined as the difference of magnitudes determined in J and K wavebands, Bulge to total luminosity ratio (B/T) and absolute magnitude. From the obtained value of total integrated magnitude, we derived the absolute magnitude of each sample galaxies using the equation given below.

$$M = m - 5\log(DL) - 5 \qquad (3.3)$$

where m is the apparent magnitude, DL is the luminosity distance in (Mpc) taken from NED, and M is the absolute magnitude. The Hubble constant of $H_0 = 73\,km\,s^{-1}/Mpc$ was used in the final conversion from arcseconds to kiloparsecs through out our analysis.

3.4   Magnitude and colour

To check the reliability of our fitting, we compared the magnitude and radius of the sample modeled by a single Sérsic function with Large galaxy atlas (LGA) data (Jarrett et al., 2003). The images were sky subtracted and available in LGA[7]. Out of the 54 galaxies in our sample, 14 galaxies were common. Figure 3.5 shows the comparison plot of our values with LGA. Jarrett et al. (2003) modeled the bulge

---

[7]http://irsa.ipac.caltech.edu/
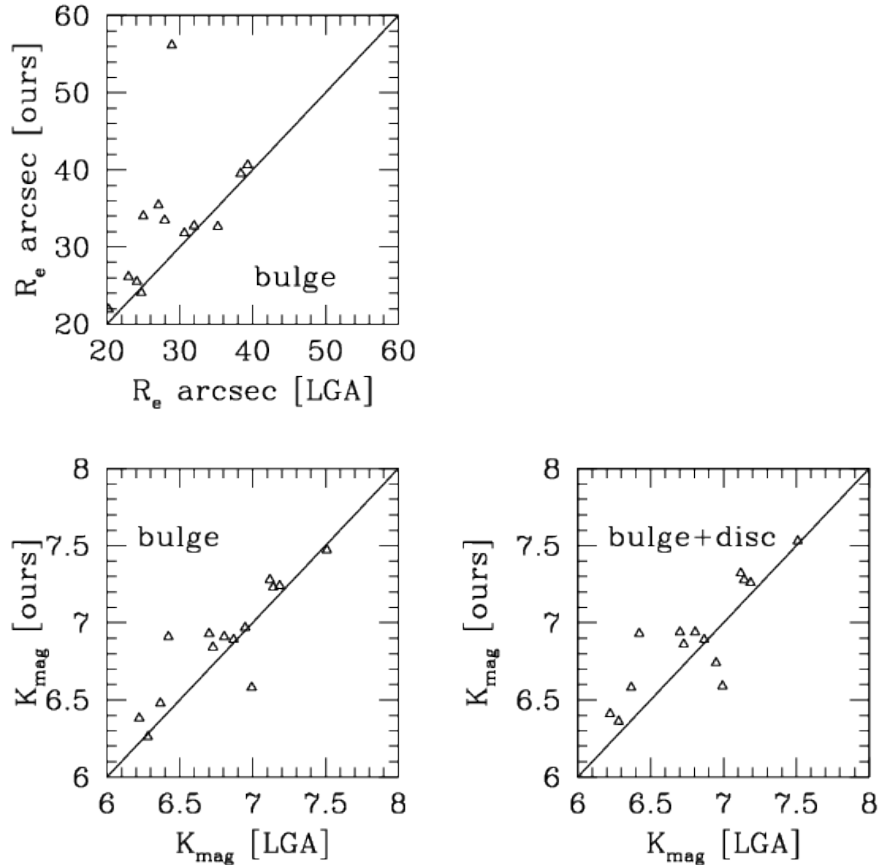
Figure 3.5: Comparison of apparent magnitude obtained from single Sérsic model (bottom left), total apparent magnitude obtained from the assumption of Sérsic and exponential model of our data with LGA sample (bottom right) and effective radii (top left) of our data with LGA sample.

component only, but we modeled with a bulge only model as well as a bulge plus disc model. In these comparison plots, no one to one relation was observed. The difference in the structural parameters determined between LGA and our decomposition can be attributed to the difference in the algorithms used. Further, LGA uses background subtracted images, while we used GALFIT to estimate the background. It is not easy to distingush the exact level of background (as in the case of K-band observation, where sky is high) from a flat long disc. As our method uses information from every pixel to determine every component of a galaxy, it is belived to provide a more realistic estimation of the structural parameters.
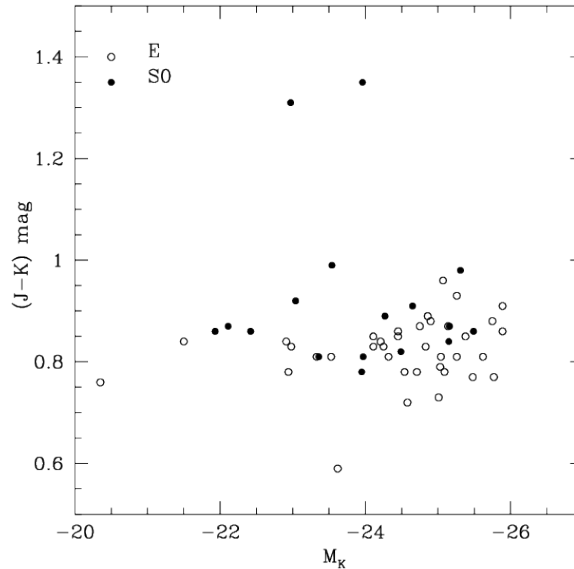
Figure 3.6: Colour-magnitude relation of our sample. Mean value of (J-K) of the sample is (0.87 ± 0.12) mag

The relation between the colour and absolute magnitude of galaxies is known as colour- magnitude (CMR) relation (Visvanathan & Sandage, 1977). $(J-K)-M_K$ is the colour-magnitude relation of NIR analysis, useful to study the average metallicity of the composite system and would be free from the contributions of the younger populations (Dressler, 1984). J-K is the near infrared colour and would be sensitive to the metallicity that corresponds to the old stellar populations. In this analysis, we plot J-K against M_K as shown in Figure 3.6. Our sample consisted of total absolute magnitude in the range of $-20.35 > M_K > -25.89$. The mean value of the colour of total sample was found to be 0.87 ± 0.12. While considering ellipticals only, the mean value was 0.84 ± 0.09, whereas for lenticulars the value was 0.93 ± 0.15.

The colour of the elliptical galaxies increases with increase in luminosity (Faber, 1973), because it is related to the mass of the galaxy. In our analysis, we identified that most of the galaxies were seen in the higher luminosity region and were scattered. Compared to cluster sample, the colour of field galaxies shows more scatter due to the effect of environment (Larson et al., 1980; Terlevich et al., 1999). Jarrett et al. (2003) studied the early type galaxies in NIR and reported the $(J-K)$ colour of early type galaxies in the range of 0.8 to 1.2. In colour magnitude diagram, the

value of $(J-K)>1$ indicates the presence of complex and dust reddened structures (Jarrett et al., 2003). In our plot NGC3607, NGC1533 and NGC4636 galaxies were identified as the three outliers. NGC4636 had value of $(J-K)$ as less than 0.8, whereas other two outliers had $(J-K)$ values greater than 1.3.

The method of finding magnitude (and colour) followed by Jarrett et al. (2003) is different. They have used elliptical aperture with 20 mag/arcsec, isophote, while ours effectively use much larger aperture. Hence one to one correspondance is not expected between the two colours. Further, one of the outlier NGC1533 is not in the sample of (Jarrett et al., 2003).

3.5   Structural parameters and their correlations

The bulge and disc structural parameters were extracted by two dimensional bulge disc decomposition. The bulge component of the sample was well fitted by Sérsic function and the disc component by exponential function. The correlation between the structural parameters of these components and the comparison with previous studies provide various clues about the formation and evolution of such systems.

3.5.1   Bulge structural parameters and correlations

The interesting piece of information from our analysis was the lower values of bulge to total luminosity ratio B/T and Sérsic index, 'n' for our sample galaxies. The distribution of B/T and n is shown in Figure 3.7a and Figure 3.7b. From the Figure 3.7a it was identified that most of the galaxies had B/T ratio less than 0.5. The light contribution of bulge compared to disc was found to be lesser. The mean value of B/T of our 2MASS sample was 0.33 ± 0.07. Similarly in case of Sérsic index we obtained less value, ie $n<2.0$. The mean value of Sérsic index from the analysis of 2MASS images was 1.19 ± 0.21.

We did not find any significant relation between Sérsic index and B/T and no significant correlation of n and B/T with any of the bulge parameters was identified.

Figure 3.8 shows the relation among bulge structural parameters. In Figure 3.8a, the effective surface brightness is positively related to the effective radius. The relation between effective radius and mean surface brightness within effective radius
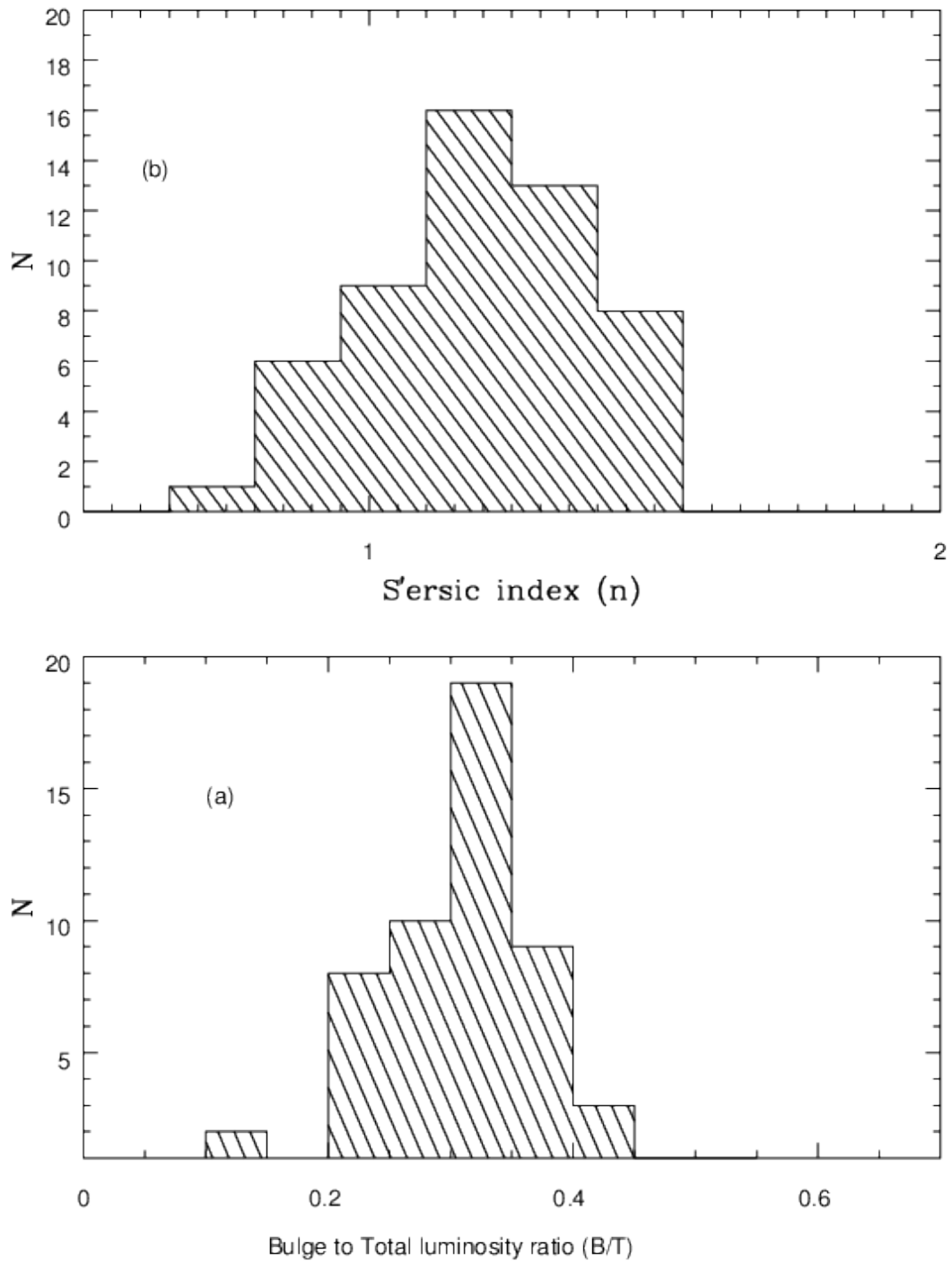
Figure 3.7: Distribution of Bulge to Total luminosity ratio B/T(a) and Sérsic index (b).

$<\mu_b(< R_e)>$ was already observed in ellipticals and bulges of galaxies reported by Kormendy (1977) known as Kormendy relation (see Section 1.8.1). Our sample satisfies the Kormendy relation with correlation coefficient of 0.66 with significance greater than 99.99%. The linear relation is expressed as,

$$<\mu_b(< R_e)> = (1.41 \pm 0.21) \log R_e + (15.0 \pm 0.06) \qquad (3.4)$$

We found that slope of the KR of our sample is comparable with that of cluster ellipticals studied in NIR K-band as reported by Ravikumar et al. (2006). Barway et al. (2009) obtained the KR for lenticular galaxies from NIR K-band that supports the fundamentally different systems of bright ($M_T < -24.5$) and faint lenticulars ($M_T > -24.5$) with different slopes. The slope obtained for bright lenticulars were similar to that of cluster ellipticals. KR reported for NIR-J band images of late type galaxies by Méndez-Abreu et al. (2010) and there was no significant difference observed for bulges of lenticular and early-to-intermediate spiral galaxies. This idea supports that bulges and ellipticals would be formed in the same way.

In Figure 3.8b, effective radius of our sample galaxies was positively correlated with the bulge luminosity which suggests that, larger the bulges the more luminous the galaxies are. The linear correlation coefficient for this relation is $r = -0.92$.

$$M_b = (-23.59 \pm 0.06) - (3.63 \pm 0.22) \log R_e \qquad (3.5)$$

Where M_b is the bulge luminosity at K-band and R_e is the bulge effective radius. Similar relation was obtained for NIR J-band images of disc galaxies (Méndez-Abreu et al., 2010). There is no significant correlations were obtained for B/T with bulge structural parameters (See Figure 3.8).

The three parameter relation of bulge effective radius R_e, mean surface brightness within effective radius, $<\mu_b(< R_e)>$ and velocity dispersion σ of bulges and elliptical galaxies are known as Fundamental plane (FP) relation (see Section 1.8.1). It is a well known relation for the study the properties of early-type galaxies. FP relation was used to estimate the galaxy mass by applying the virial theorem. We
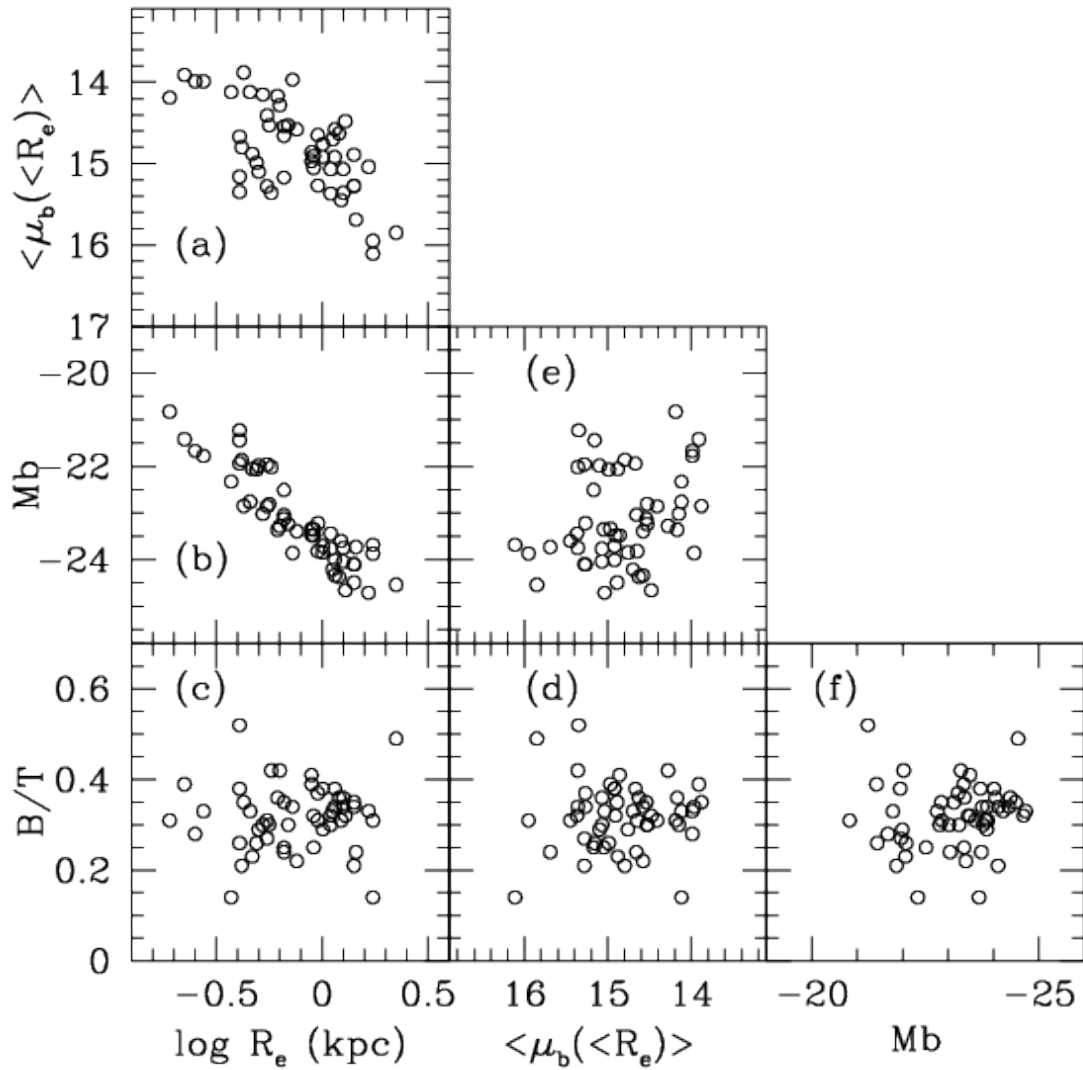
Figure 3.8: Correlations among bulge structural parameters. R_e is the effective radius, M_b is the bulge luminosity, $< \mu_b(< R_e) >$ mean surface brightness with in effective radius and B/T is the bulge to total luminosity ratio.
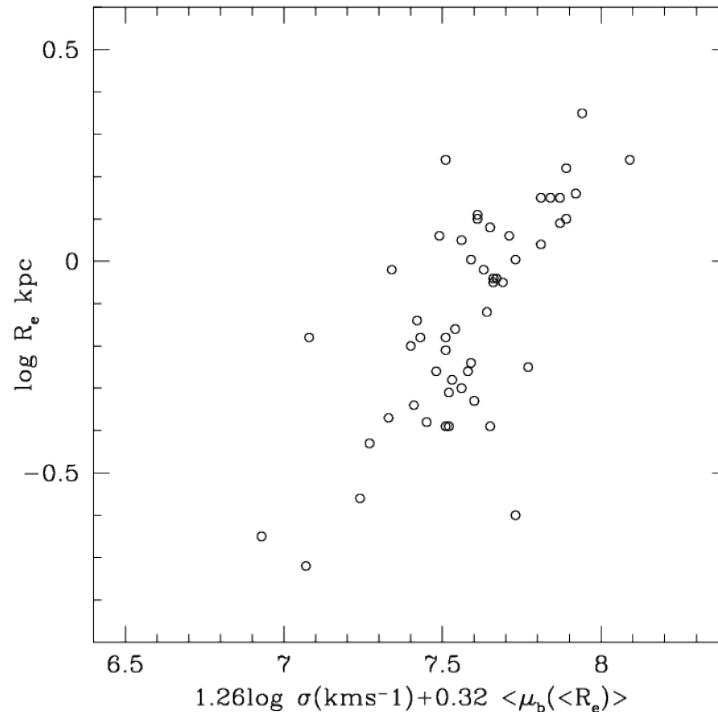
Figure 3.9: Three parameter scaling relation of R_e, the effective radius, $<\mu_b(e)>$ mean surface brightness with in effective radius and σ, the central velocity dispersion.

derived the FP relation for our sample galaxies as shown in Figure 3.9. The central velocity dispersion σ value were retrieved from the on line HyperLeda catalog (Paturel et al., 2003).

The FP coefficients describing our sample is expressed as,

$$\log R_e = (1.26 \pm 0.18) \log \sigma + (0.32 \pm 0.03)<\mu_b(e)> - (7.72 \pm 0.54) \qquad (3.6)$$

The coefficients were estimated by using the least square minimization method and errors were calculated by the bootstrapping method. The coefficients of $\log \sigma$ and $<\mu_b(e)>$ of our early-type galaxies were compared with coma cluster ellipticals studied by Pahre et al. (1995) and Mobasher et al. (1999). Pahre et al. (1995)
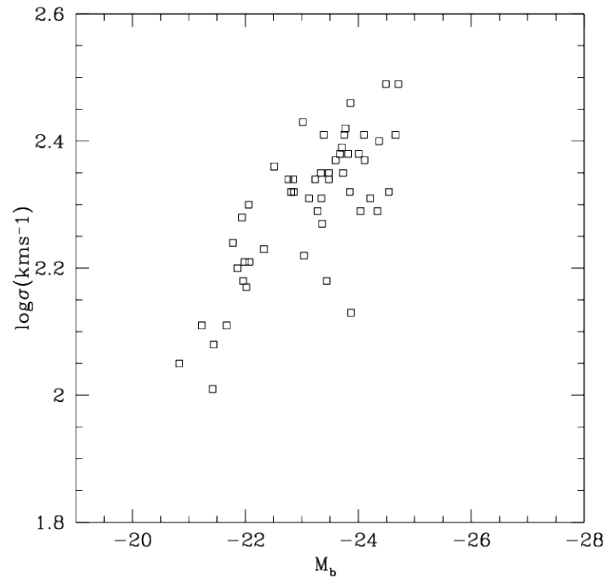
Figure 3.10: Variation of bulge luminosity M_b in K-band and velocity dispersion σ.

obtained the FP relation for 12 ellipticals from coma cluster studied in V band as

$\log R_e = (1.33 \pm 0.19) \log \sigma + (0.30 \pm 0.03) <\mu_b(_e)> + c$ and

Mobasher et al. (1999) obtained FP relation for 48 elliptical galaxies studied in NIR K-band and the relation was,

$\log R_e = (1.38 \pm 0.26) \log \sigma + (0.30 \pm 0.02) <\mu_b(_e)> + c$ respectively.

Pahre et al. (1995) studied the FP relation of galaxies in NIR and was obtained as

$\log R_e = (1.32 \pm 1.50) \log \sigma + (0.30 \pm 0.32) <\mu_b(_e)> + c.$

From these relations it was observed that our coefficients are consistent within the errors of others study. It was also inferred that the FP relation of our sample galaxies are comaparable with the coma cluster ellipticals. The variations of coefficients for FP could be related to various factors of fitting methods, wavelength dependence, sample selection, etc. Our samples resides in low density environment (Annibali et al., 2010), but the analysis could not identify any difference in coefficients of KR and FP with cluster sample.

Luminosity of the bulges of galaxies related to the central velocity dispersion,

was one of the projections of fundamental plane relation reported by Faber & Jackson (1976) known as FJ relation (see Section 1.8.1). Figure 3.10 shows a plot of FJ relation and can be represented as,

$$M_b = (0.49 \pm 0.32) \log \sigma - (0.07 \pm 0.01) \qquad (3.7)$$

The linear correlation coefficient (r) of the FJ relation is obtained to be -0.65 with a significance greater than 99.99%.

where σ is the central veocity dispersion and M_b is the bulge luminosity. The slope value (0.49 ± 0.32) is consistent with the value of (0.4 ± 0.3) obtained for J-band data reported by Méndez-Abreu et al. (2010).

3.6 Correlations of disc structural parameters

The relation between the disc structural parameters are shown in Figure 3.11. In Figure 3.11a, it can be seen that the distribution of central disc brightness with disc scale length have large scatter. But it can be seen that the galaxies having more disc component exhibit fainter central surface brightness of disc. The correlation between these two parameters in our sample was very poor as 0.47 with significance 99.96%. The linear relation is expressed as,

$$\mu_d(0) = 16.21 \pm 0.11 + (1.09 \pm 0.25) \log(R_d/kpc) \qquad (3.8)$$

In the case of spiral galaxies in NIR were studied byMöllenhoff & Heidt (2001) obtained the relation was,

$$\mu_d(0) = 16.6 + (2.02 \pm 0.64) \log(R_d/kpc). \ (3.9)$$

The coefficients obtained for J-band data of disc galaxies reported by Méndez-

| Galaxy | J | K | $J-K$ | R_e | R_d | n |
Name	(mag)	(mag)	(mag)	(arcsec)	(arcsec)	
NGC 0128	9.52	8.53	0.98	8.17	20.48	1.31
NGC 0777	9.32	8.19	1.12	5.11	16.45	1.08
NGC 1052	8.33	7.48	0.85	4.96	16.67	1.20
NGC 1209	9.19	8.32	0.87	5.12	18.52	1.11
NGC 1366	9.90	9.03	0.87	2.40	9.96	0.72
NGC 1380	7.77	6.89	0.88	7.89	28.83	1.38
NGC 1389	9.44	8.57	0.87	5.62	13.05	1.28
NGC 1407	7.67	6.94	0.73	8.59	28.17	1.31
NGC 1426	9.33	8.54	0.79	4.91	15.87	1.25
NGC 1521	9.52	8.58	0.94	4.97	19.14	1.07
NGC 1533	8.49	7.19	1.30	5.30	21.91	1.06
NGC 1553	7.18	6.36	0.82	5.27	22.90	0.91
NGC 1947	8.34	7.53	0.81	7.46	19.61	1.54
NGC 2749	9.80	8.92	0.89	4.58	13.24	1.12
NGC 2962	9.61	8.62	0.99	3.17	18.85	0.86
NGC 3136	8.11	7.32	0.79	6.07	26.52	1.42
NGC 3268	9.01	8.23	0.79	4.94	20.44	1.16
NGC 3489	8.28	7.44	0.84	4.99	19.69	1.34
NGC 3557	8.12	7.26	0.87	6.34	23.37	1.25
NGC 3607	7.94	6.59	1.35	6.88	19.78	1.24
NGC 3818	9.69	8.86	0.84	3.59	15.51	1.04
NGC 3962	8.39	7.63	0.76	7.37	24.11	1.51
NGC 4374	7.22	6.41	0.81	7.78	24.52	1.24
NGC 4552	7.69	6.86	0.84	5.90	20.40	1.34
NGC 4636	7.52	6.93	0.59	7.58	24.75	1.06

Table - continued.

Galaxy Name	J (mag)	K (mag)	$J - K$ (mag)	R_e (arc sec)	R_d (arc sec)	n
NGC 4696	8.06	7.28	0.78	8.88	26.79	1.39
NGC 4697	7.30	6.58	0.72	8.11	28.42	1.46
NGC 5011	8.88	8.09	0.78	4.55	15.77	1.17
NGC 5044	8.46	7.66	0.81	7.99	21.25	1.01
NGC 5077	9.05	8.13	0.92	5.49	16.64	1.10
NGC 5090	8.51	7.62	0.89	6.38	28.88	1.16
NGC 5193	9.55	8.68	0.88	3.73	10.86	0.93
NGC 5266	8.46	7.59	0.87	5.86	24.07	1.35
NGC 5328	9.28	8.46	0.82	4.58	15.16	1.08
NGC 5363	7.79	6.89	0.91	6.1	22.01	1.23
NGC 5638	9.09	8.28	0.8	4.48	13.71	1.05
NGC 5812	8.80	7.95	0.85	4.79	17.11	1.23
NGC 5831	9.26	8.45	0.81	4.61	13.77	1.11
NGC 5846	7.89	6.74	1.15	10.99	28.03	1.49
NGC 5898	8.91	8.07	0.83	4.69	15.35	1.20
NGC 6721	9.82	8.89	0.94	3.83	12.83	1.05
NGC 6758	9.13	8.32	0.81	5.17	16.25	1.32
NGC 6776	9.88	9.02	0.86	3.17	10.14	0.87
NGC 6868	8.26	7.49	0.77	6.44	21.18	1.28
NGC 6875	9.79	8.89	0.89	4.64	11.54	0.53
NGC 6958	9.27	8.41	0.86	3.42	12.99	0.95
NGC 7097	9.51	8.68	0.83	3.27	10.83	0.93
NGC 7135	9.65	8.83	0.81	3.77	18.00	1.16
NGC 7332	8.97	8.05	0.91	3.29	17.75	1.04
NGC 7377	9.01	8.16	0.85	8.02	24.96	1.42
IC 1459	7.73	6.94	0.79	5.94	22.83	1.29
IC 2006	9.33	8.49	0.84	4.40	12.41	1.10
IC 3370	8.76	7.89	0.87	6.57	18.56	1.34
IC 5063	9.62	8.72	0.89	4.91	13.83	1.36

Table 3.1: Measured parameters of galaxies (1) Host galaxy name; (2) Total apparent magnitude in J band (3) Total apparent magnitude in K band (4) (J-K) colour (5) Effective radius; R_e in arc sec (6) Disc scale length; R_d in arc sec and (7)Sérsic index; n

Galaxy Name	μ_b (mag)	$<\mu_b(<R_e)>$ (mag arcsec^{-2})	μ_d (mag)	M_b	M_d	M_K	B/T
NGC 0128	14.19	15.86	17.82	-24.54	-24.57	-25.31	0.49
NGC 0777	13.79	15.05	16.86	-24.71	-25.44	-25.89	0.33
NGC 1052	12.85	14.31	15.98	-22.86	-23.7	-24.11	0.31
NGC 1209	13.54	14.85	17.22	-23.48	-23.88	-24.45	0.41
NGC 1366	13.53	14.19	16.43	-20.83	-21.69	-22.11	0.31
NGC 1380	12.94	14.73	16.59	-23.85	-24.77	-25.16	0.29
NGC 1389	13.63	15.24	16.80	-21.23	-21.12	-21.93	0.52
NGC 1407	13.15	14.81	16.35	-23.39	-24.73	-25.01	0.22
NGC 1426	13.59	15.14	17.13	-22.02	-22.34	-22.94	0.42
NGC 1521	14.02	15.26	17.48	-24.11	-24.81	-25.26	0.34
NGC 1533	12.78	13.99	16.33	-21.78	-22.53	-22.97	0.33
NGC 1553	13.16	14.12	15.31	-22.33	-24.33	-24.49	0.14
NGC 1947	13.21	15.29	16.34	-21.96	-23.01	-23.36	0.27
NGC 2749	14.03	15.36	16.98	-23.75	-24.43	-24.9	0.34
NGC 2962	13.92	14.80	17.25	-21.86	-23.28	-2.54	0.21
NGC 3136	12.67	14.53	16.82	-23.24	-24.15	-24.54	0.30
NGC 3268	13.52	14.91	17.19	-23.48	-24.28	-24.71	0.32
NGC 3489	12.19	13.91	16.43	-21.42	-21.88	-22.42	0.39
NGC 3557	12.93	14.49	16.52	-24.66	-25.46	-25.89	0.32
NGC 3607	12.35	13.88	15.55	-22.85	-23.48	-23.96	0.35
NGC 3818	13.48	14.67	17.34	-21.94	-22.45	-22.98	0.38
NGC 3962	12.94	14.97	17.09	-23.34	-23.81	-20.35	0.39
NGC 4374	12.62	14.16	15.74	-23.02	-23.93	-24.32	0.30
NGC 4552	12.05	13.76	15.91	-20.44	-20.99	-21.5	0.37
NGC 4636	13.66	14.88	16.18	-22.06	-23.33	-23.62	0.23

Table - continued.

Galaxy Name	μ_b (mag)	$<\mu_b(<R_e)>$ (mag arcsec^{-2})	μ_d (mag)	M_b	M_d	M_K	B/T
NGC 4696	14.29	16.11	16.58	$-23..68$	-25.6	-25.77	0.14
NGC 4697	12.72	14.66	16.14	-23.04	-24.28	-24.58	0.24
NGC 5011	13.24	14.65	16.48	-23.82	-24.69	-25.09	0.31
NGC 5044	14.56	15.69	16.59	-23.73	-24.96	-25.26	0.24
NGC 5077	13.63	14.92	16.80	-23.71	-24.23	-24.75	0.38
NGC 5090	13.89	15.29	17.19	-24.1	-25.48	-25.75	0.21
NGC 5193	14.06	15.05	16.21	-23.35	-24.51	-24.83	0.25
NGC 5266	12.85	14.58	16.95	-24.34	-25.04	-25.49	0.34
NGC 5328	13.63	14.89	16.83	-24.49	-25.15	-25.65	0.35
NGC 5363	12.60	14.12	16.16	-22.76	-23.51	-23.95	0.33
NGC 5638	13.79	14.99	16.29	-22.07	-23.21	-23.53	0.26
NGC 5812	12.76	14.28	16.71	-23.28	-23.61	-24.21	0.42
NGC 5831	13.79	15.10	16.52	-21.99	-22.95	-23.33	0.29
NGC 5846	13.47	15.46	16.64	-23.6	-24.45	-24.86	0.31
NGC 5898	13.08	14.54	16.48	-23.13	-23.77	-24.25	0.35
NGC 6721	13.87	15.07	16.79	-23.77	-24.68	-25.07	0.30
NGC 6758	13.24	14.92	16.89	-24.01	-24.52	-25.05	0.38
NGC 6776	13.80	14.7	16.49	-24.21	-24.93	-25.38	0.33
NGC 6868	13.03	14.64	16.60	-24.37	-24.99	-25.48	0.36
NGC 6875	14.91	15.28	16.72	-23.22	-23.76	-24.27	0.37
NGC 6958	13.13	14.17	16.46	-23.36	-23.96	-24.45	0.36
NGC 7097	13.54	14.54	16.24	-22.81	-23.71	-24.11	0.30
NGC 7135	13.78	15.18	17.43	-22.51	-23.65	-23.97	0.25
NGC 7332	12.80	13.99	16.65	-21.67	-22.67	-23.04	0.28
NGC 7377	14.09	15.95	17.54	-23.87	-24.75	-25.15	0.31
IC 1459	12.35	13.97	16.18	-23.86	-24.58	-25.03	0.34
IC 2006	13.87	15.16	16.26	-21.44	-22.59	-22.91	0.26
IC 3370	13.36	15.07	16.72	-24.04	-24.65	-25.14	0.36
IC 5063	13.62	15.37	16.84	-23.44	-24.22	-24.65	0.32

Table 3.2: Properties of the sample. (1) Host galaxy name; (2) μ_b central bulge surface brightness (3) $<(\mu_b(<R_e)>$ is effective surface brightness with in R_e (4)μ_d is the disc central surface brightness (5) M_b is bulge luminosity (6)M_d is disc luminosity(7)M_K is the total luminosity and (8) (B/T) is bulge to total luminosity ratio
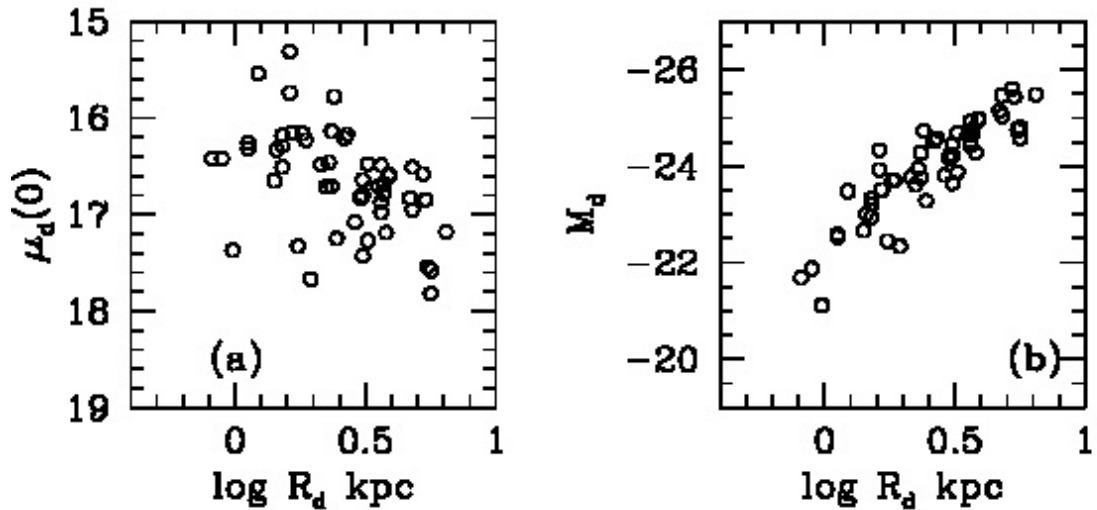
Figure 3.11: Correlations of disc scale length with central surface brightness and disc luminosity

Abreu et al. (2010) were (17.36 ± 0.1) and (1.4 ± 0.2). Similar relation between the central surface brightness and disc scale length were observed in bright and faint lenticulars (Barway et al., 2009; Noordermeer & van der Hulst, 2007). The positive relation between disc scale length and disc luminosity in Figure 3.11b suggests that more luminous discs had larger sizes of the disc component.

3.7 Correlations between bulge and disc

Our sample shows a strong correlation between the bulge effective radius and disc scale length as shown in Figure 3.12. The larger discs were found to be residing in the larger bulges (see Figure 3.12.a). The linear correlation coefficient obtained was 0.94 with a significance greater than 99.99%. Similar correlations were reported earlier for late type galaxies (Courteau et al., 1996; Möllenhoff & Heidt, 2001). The bulges would be formed in such systems from the already existing disc, which supports the secular evolution of bulges. The luminosities of bulge and disc also well correlated (see Figure 3.12.b). The central surface brightness of disc and effective radius of bulge are also related as shown in Figure 3.12.c.
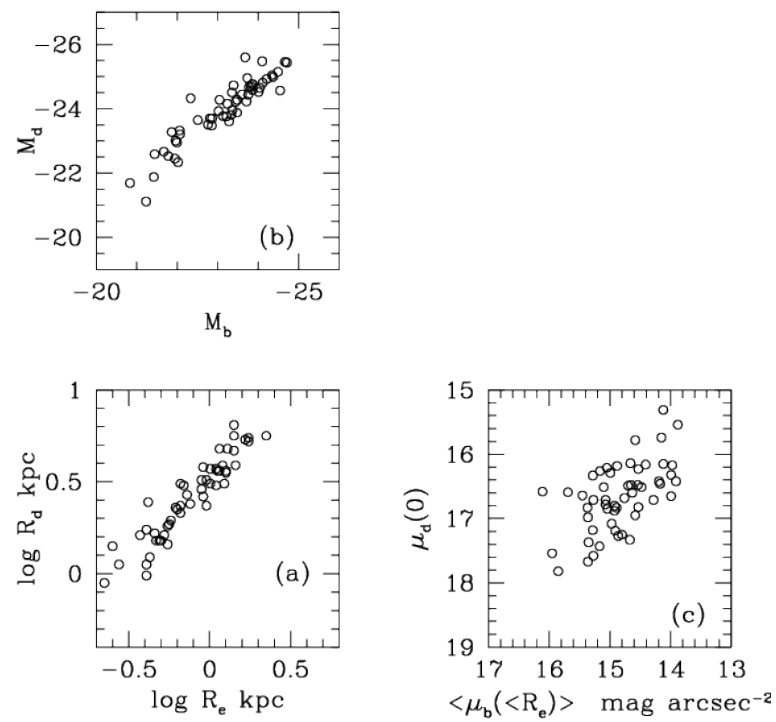
Figure 3.12: Correlations between the bulge and disc parameters: Relation between bulge effective radius and disc scale length(a), Relation between the bulge and disc luminosities(b) and Relation between the bulge effective surface brightness and central disc surface brightness (c)

.

3.8   Summary

We performed the bulge disc decomposition and isophotal fitting of 54 early-type galaxies obtained from the NIR observation of 2MASS. The two dimensional decomposition was done by the code GALFIT. We used Sérsic and exponential functions for modeling the 37 ellipticals and 17 lenticulars. From our analysis, we identified that all sample galaxies had Sérsic index less than 2 and the value of B/T less than 0.5. Further analysis needs to be done on the detectable disc component present in ellipticals to identify whether it is physically meaningful or not. The shallowness of 2MASS observations may affect our result on the significance of disc component detected. The presence of significant disc component in the sample galaxies including 20 ellipticals was inferred. The relation between the disc structural parameters are comparable with that obtained for late type systems mentioned in literature which supports the presence of disc present in our early-type sample. It appeared that the component in the galaxies was better detected in NIR observation in comparison with Optical. The positive correlation between the effective radius and disc scale length supports the finding that larger galaxies have larger discs. From the scaling relations of KR, FJ and FP along with the comparisons carried out with the values available in literature, we found that the sample galaxies follow the similar scaling relations as that of cluster samples. It supports the inference that the bulges of early type galaxies observed in the field were fomed in the same way as that of the cluster sample.

We performed the two dimensional image analysis on the same galaxies in more better observations by Spitzer.

In the next chapter, we report the photometric analysis of the same sample in deeper observational data from Spitzer.

Chapter 4

Photometric analysis of early-type galaxies in Mid infrared images using Spitzer observations

4.1 Introduction

Structural information of galaxies can be extracted by the technique of surface photometry. In the previous chapter, we discussed about the photometric structural analysis of early-type galaxies observed in NIR K-band. From the relation between structural parameters of galaxies, we identified significant disc component in majority of the sample galaxies. The correlation analysis of structural parameters revealed that, the detectable disc component present in the sample had similar properties of disc galaxies, and were comparable to previous studies. However, the analysis used shallow images from 2MASS. In this chapter, we analyze the same galaxies observed by *Spitzer* in mid-IR 3.6 μm band. The effect of sky extinction in IRAC 3.6 μm was weaker than that of 2MASS K band (Gao et al., 2009). The radiations obtained from 2MASS K band and Spitzer 3.6 μm were dominated by old stellar populations. But the effect of sky extinction and reddening was very weak in IRAC 3.6 μm wavelength. Spitzer 3.6 μm band was treated as a good stellar mass tracer of nearby galaxies (Fazio et al., 2004). Minimal effect of dust and stellar population for Spitzer 3.6 μm band compared to optical band may help to study the structural

information of galaxies (Fisher & Drory, 2010). We mainly focused on the analysis of structural properties of bulges and discs present in our sample galaxies. The correlation between bulge and disc structural parameters were also studied.

4.2 Analysis and Results

We performed the isophotal fitting and two dimensional bulge disc decomposition on sample galaxies observed in 3.6 μm wavelength. Out of 54 galaxies studied in 2MASS, observations from Spitzer were available for 39 galaxies. The same procedure of data analysis technique used for 2MASS data were repeated for these images also. The two dimensional bulge disc decomposition done by GALFIT, required guess values as input. The input parameters of apparent magnitude, effective radius, disc scale length and center of galaxy were obtained by ellipsefit method. Ellipsefit were performed on these images with IRAF software described in Section 2.4. For Spitzer images we used the images of point spread function (PSF) and uncertainty images, which were not used in 2MASS analysis. PSF image were created by GALFIT described in Chapter 2 (See Section 2.5). The uncertinity images were obtained from the output of MOPEX software package provided by *Spitzer* (see Section 2.5).

4.2.1 Photometric structural parameters

By the two dimensional bulge disc decomposition analysis, we obtained the structural parameters of bulge and disc. The measured and estimated parameters were shown in Table 4.1. Out of 39 galaxies we excluded 5 galaxies (NGC1553, NGC3489, NGC3962, NGC4697 and NGC5011) due to bad fit.

Recently many of the structural studies (Gadotti, 2009; Vaghmare et al., 2013; Fernández Lorenzo et al., 2014; Krajnović et al., 2011; Fisher & Drory, 2010) suggested, Sérsic index, n as one of the parameters to identify the bulge type. Structural studies of galaxies observed in optical band Gadotti (2009) and Krajnović et al. (2011) used $n = 2$ for differentation of the bulge types as classical or pseudo bulge. In the case of isolated galaxies studied in optical band Fernández Lorenzo et al. (2014) used $n = 2.5$ for differentiating the bulges. Studies about pseudo bulges in

Galaxy Name	R_e (kpc)	n	R_d (kpc)	μ_b (mag)	μ_d (mag)	$< \mu_b(< R_e) >$ (mag arcsec^{-2})	M_b	M_d	B/T	R_e/R_d
N0777	4.95	2.45	14.5	14.03	20.43	17.86	-24.26	-24.02	0.55	0.34
N1052	4.53	4.8	2.72	10.23	19.71	18.81	-23.06	-21.05	0.86	1.66
N1209	2.02	2.14	7.38	14.19	20.42	17.41	-22.71	-22.52	0.54	0.27
N1366	0.27	1.28	1.47	14.37	18.91	15.98	-19.7	-20.52	0.33	0.18
N1380	7.43	4.04	8.35	11.89	20.75	18.91	-24.02	-22.43	0.81	0.89
N1389	1.24	2.7	3.59	13.98	22.61	18.3	-20.74	-18.74	0.86	0.34
N1407	3.16	2.2	10.7	14.35	19.86	17.68	-23.41	-23.88	0.39	0.29
N1426	1.63	2.97	5.04	13.42	21.06	18.27	-21.37	-21.03	0.57	0.32
N1533	0.53	1.23	2.38	15.58	19.33	17.1	-20.11	-21.13	0.28	0.22
N1553	11.3	6.25	2.83	8.623	18.55	20.21	-23.66	-22.37	0.77	4.01
N1947	5.3	3.81	45.8	12.96	24.5	19.51	-22.68	-22.37	0.57	0.11
N2962	0.57	1.43	4.09	14.74	19.56	16.62	-20.76	-22.08	0.22	0.14
N3489	0.44	2.39	1.62	12.55	18.99	16.26	-20.54	-20.63	0.47	0.27
N3557	3.22	1.84	11.5	14.59	19.51	17.23	-23.91	-24.41	0.38	0.27
N3607	1.44	2.52	4.79	13.42	20.16	17.38	-22.98	-21.82	0.54	0.3
N3818	0.71	2.01	3.51	13.91	20.04	16.87	-20.96	-21.27	0.42	0.2
N3962	3.04	2.78	42.8	13.54	21.81	18.01	-22.98	-24.93	0.14	0.07
N4374	1.4	2.1	6.08	15.72	24.05	18.87	-20.46	-18.46	0.86	0.23
N4636	1.62	2.08	6.89	14.68	20.05	17.79	-21.85	-22.72	0.31	0.23
N4697	11.1	4.9	9.68	11.08	21.71	19.87	-23.93	-21.81	0.87	1.14

Table - continued.

Galaxy Name	R_e (kpc)	n	R_d (kpc)	μ_b (mag)	μ_d (mag)	$<\mu_b(<R_e)>$ (mag arcsec^{-2})	M_b	M_d	B/T	R_e/R_d
N5011	0.57	0.8	5.02	17.68	20.03	18.47	−18.94	−22.07	0.05	0.11
N5044	4.51	1.71	14.6	15.97	20.46	18.37	−23.5	−23.97	0.39	0.3
N5077	2.24	2.07	7.38	14.33	19.98	17.42	−22.94	−22.96	0.49	0.3
N5090	3.03	1.86	15.02	15.04	19.95	17.72	−23.3	−24.54	0.24	0.2
N5363	2.72	1.22	2.65	21.18	22.04	22.69	−18.07	−18.65	0.36	1.02
N5638	1.21	1.89	3.44	14.82	19.31	17.56	−21.43	−21.95	0.38	0.35
N5812	1.35	2.23	5.99	13.37	19.94	16.77	−22.48	−22.53	0.48	0.22
N5831	1.44	2.85	3.72	13.27	19.79	17.88	−21.5	−21.65	0.47	0.38
N5846	5.56	2.63	21.1	14.49	21.41	18.68	−23.64	−23.8	0.46	0.26
N6776	2.69	2.24	11.5	13.73	19.98	17.15	−23.64	−23.97	0.42	0.23
N6868	4.22	2.56	18.8	13.68	20.82	17.72	−24.01	−24.16	0.46	0.22
N6958	1.02	1.99	4.66	13.28	19.17	16.22	−22.44	−22.77	0.42	0.21
N7097	1.31	2.43	4.07	13.21	19.28	17	−22.18	−22.36	0.45	0.32
N7135	1.27	2.63	6.57	13.31	20.11	17.49	−21.64	−22.58	0.29	0.19
N7332	0.92	3.91	2.86	10.44	19.67	17.2	−21.22	−21.2	0.5	0.32
IC1459	2.27	3.01	8.28	12.03	19.75	16.97	−23.4	−23.42	0.49	0.27
IC2006	1.39	2.82	2.35	13.59	19.46	18.15	−21.15	−20.99	0.53	0.58
IC3370	6.38	3.33	16.4	13.03	21.94	18.62	−24.02	−22.74	0.76	0.38
IC5063	3.71	3.04	9.84	13.13	20.82	18.12	−23.33	−22.76	0.62	0.37

Table 4.1: Properties of the sample. (1) Host galaxy name; (2) effective radius in kpc (3) Sérsic index, n (4) Disc scale length in kpc (5) central bulge surface brightness (6) Central disc surface brightness (7) Average surface brightness with in effective radius (8)Bulge luminosity (9) Disc luminosity (10) bulge to toatl luminosity ratio (11) and Ratio of effective radius to disc scale length

S0 and Sa galaxies in Mid-IR by Vaghmare et al. (2013) and E-Sd galaxies were studied by Fisher & Drory (2010) used $n = 2$ for identification the bulge type.

Our sample galaxies exhibited bulge Sérsic index in the range of 1.23 to 4.8 and the mean value of Sérsic index was analysed as 2.5. The distribution of Sérsic index is shown in Figure 4.1a. We used the mean value of Sérsic index $n = 2.5$ to divide the sample into two groups.

Another important parameter, the bulge fraction of sample galaxies was represented as B/T ratio. The distribution of B/T was within the range of 0.22 to 0.96 as shown in Figure 4.1.b. We got the mean value of B/T as 0.49. Many recent studies reported the positive correlation of n and B/T (Graham, 2001; Liu et al., 2008; Barway et al., 2009; Fernández Lorenzo et al., 2014; Vika et al., 2014).

4.3   Properties of Bulge structural parameters

In Figure 4.2, we plot the Sérsic index n as a function of B/T ratio. From this plot we found that larger Sérsic index was exhibited by galaxies with more bulge contribution. The correlation coefficient of this relation was found to be 0.61 with a significance of 99.96%. The horizontal line represents the mean value of Sérsic index 2.5, that divide our sample into two groups. We assumed galaxies with $n>2.5$ are dominanted by classical bulges and the other group $n<2.5$ is dominated by pseudobulges. Pseudo-bulges and classical bulges represent two distinct classes of objects (Kormendy & Kennicutt, 2004). For pseudobulge galaxies, the correlation between n and B/T was 0.68 with a significance of 99.47%. One of the galaxy NGC4374 with B/T ratio as 0.86 and $n = 2.1$ was avoided to find the correlation coefficient. The relation between Sérsic index and B/T were used to identify the bulge type present in the galaxies (Liu et al., 2008). The positive relation of n and B/T were used to distingush the bulge type as pseudobulge and classical bulges (Durbala et al., 2008; Weinzirl et al., 2009; Laurikainen et al., 2010). In Figure 4.2 we found that the scatter was more for galaxies with higher Sérsic index, $n>2.5$ than that for pseudobulges ($n<2.5$). Positive correlation between n and B/T was more significant in pseudobulge galaxies rather than classical bulges were already reported by Gadotti (2009) and Fisher & Drory (2008). When the contribution of bulge increases, the Sérsic index also statistically increase (Liu et al., 2008). Barway
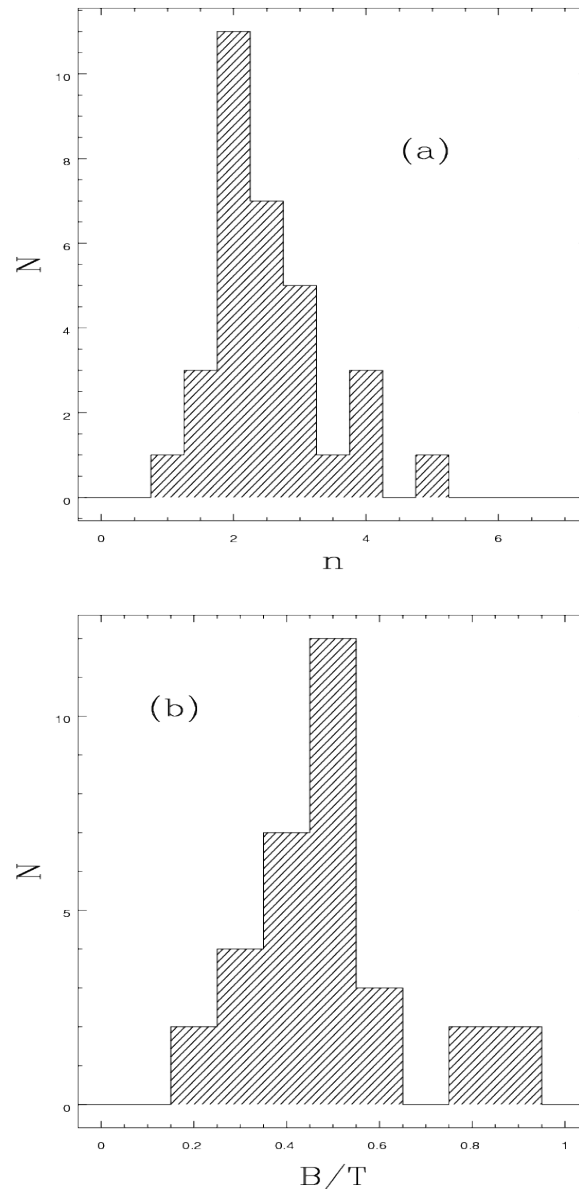
Figure 4.1: Distributions of Sérsic index and Bulge to total luminosity ratio. The value of bulge Sérsic index (top) varies from 1.23 to 4.8 and the mean value of Sérsic index n is 2.50. Distribution of the value of bulge to total luminosity ratio (bottom) varies from 0.22 to 0.96 and the mean value of B/T is 0.49

.
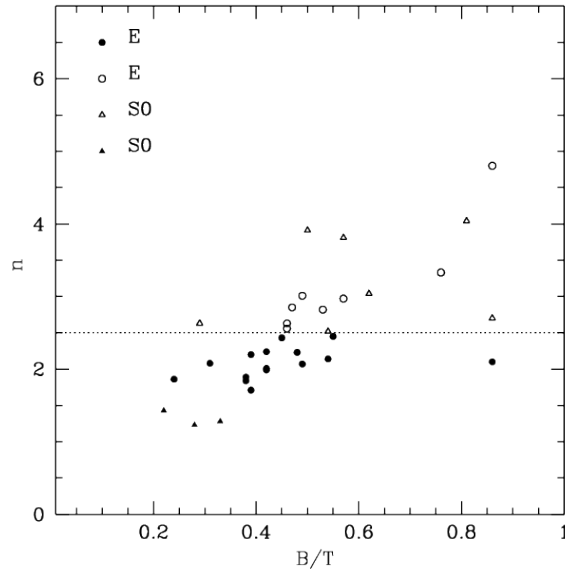
Figure 4.2: Relation between Sérsic index and Bulge to total luminosity ratio. The positive correlation (r=0.61) of bulge Sérsic index with bulge to total luminosity ratio.

et al. (2009) observed a strong relation between n and B/T for bright lenticular galaxies studied in near infrared and weak relation for faint lenticulars .

Figure 4.3 shows the relation between the bulge structural parameters. Relation between effective radius against mean surface brightness with in effective radius of sample galaxies is shown in Figure 4.3a. This is the projection of fundamental plane ralation Djorgovski & Davis (1987); Dressler et al. (1987) known as Kormendy relation Kormendy (1977)(See Section 1.8). Kormendy relation of the total sample is expressed as

$$<\mu_b(<R_e)> = (1.68 \pm 0.26) \log R_e + (17.20 \pm 0.12) \tag{4.1}$$

KR of pseudo-bulges of our sample galaxies is expressed as,

$$<\mu_b(<R_e)> = (1.35 \pm 0.33) \log R_e + (17.05 \pm 0.18) \tag{4.2}$$
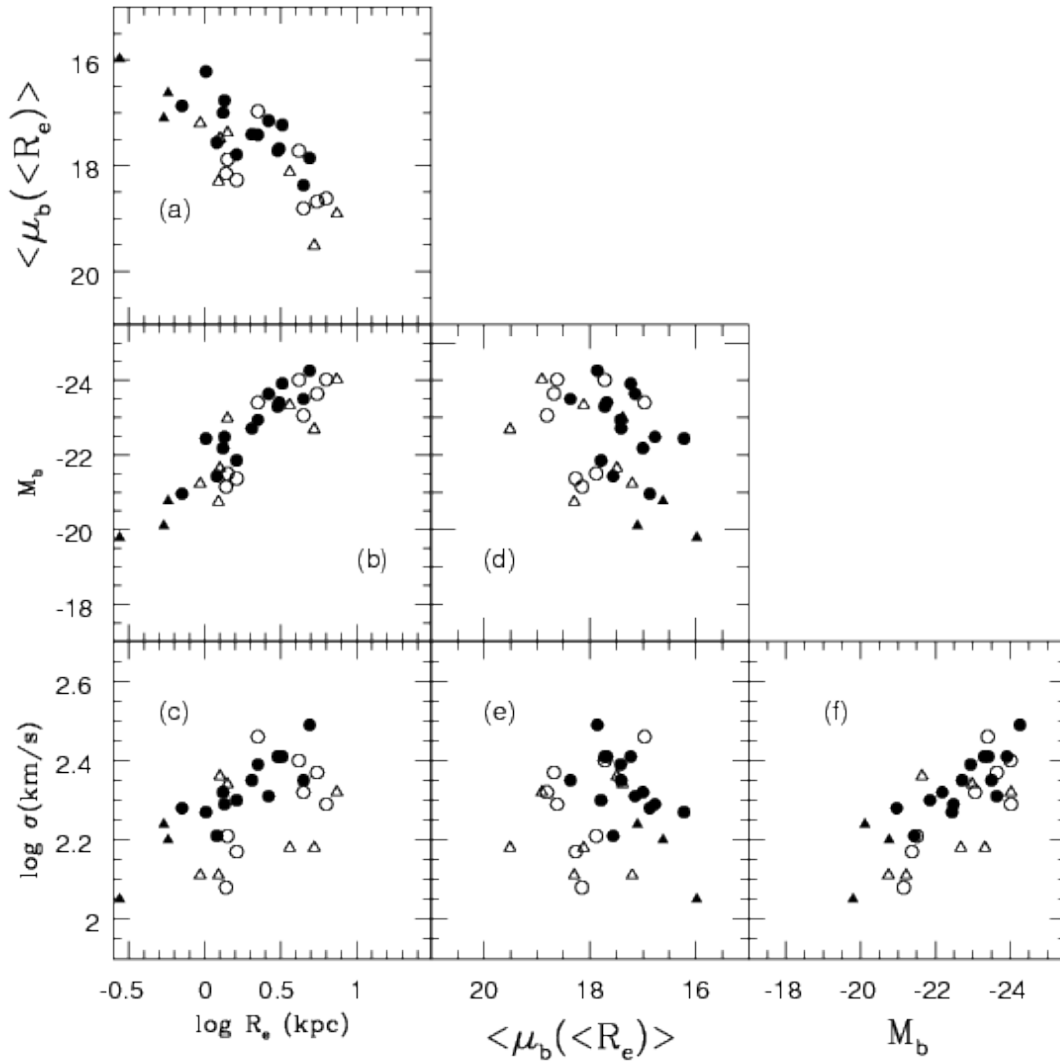
Figure 4.3: The relation between bulge structural parameters. Pseudo-bulges and classical bulges are showing different relations between the bulge structural parameters.

The relation for classical bulges of our sample is expressed as,

$$<\mu_b(_e)> = (1.38 \pm 0.32) \log R_e + (17.57 \pm 0.19) \qquad (4.3)$$

The Kormendy relation in ellipticals and classical bulges of galaxies was expected to be similar (Kormendy, 1977), but different in pseudobulges. Gadotti (2009) studied the galaxies observed in optical band, differentiated the classical bulges and pseudobulges based on the position of galaxies present in KR. The obtained pseudobulges had the value of Sérsic index $n = 2$. Vaghmare et al. (2013) also used KR to identify the pseudo bulges present in S0 galaxies observed in Mid-IR images and obtained the similar conclusion. The pseudobulges are structurally different (Kormendy & Kennicutt, 2004) and lay below the ellipticals. Classical bulges follows the same relation as that of ellipticals (Gadotti, 2009; Carollo, 1999). Our sample consists of mixed morphology, but we couldn't differentiate pseudobulges and classical bulges from the relation. A larger sample is required to improve the result. Larger galaxies would be more luminous (see Figure 4.3.b) with low surface brightness.

Figure 4.3.c depicts the relation of bulge effective radius with velocity dispersion. The bulge size of sample galaxies were positively related to their velocity dispersion. Which indicate that massive galaxies had higher velocity dispersion. These massive galaxies contain mainly older stellar populations (Gallazzi et al., 2005). Figure 4.3.d. shows that more luminous galaxies have lesser surface brightness. FJ relation is shown in Figure 4.3.f. The correlation coefficient between bulge luminosity and velocity dispersion is obtained as (r=-0.64) with a significance of 99.99%. As shown in Figure 4.3.e the surface brightness of pseudobulges exhibit a relation with velocity dispersion where as the classical bulges show no distinct relationship.

FP relation is the plane relation that connects the effective radius, mean surface brightness and velocity dispersion. This three parameter relation helped to study the galaxy formation and evolution. We studied the FP relation of sample galaxies

in mid IR and obtained the plane relation as,

$$\log \sigma = (1.36 \pm 0.26) \log R_e + (0.27 \pm 0.04) < \mu_b(< R_e) > -(7.77 \pm 1.17)$$

The coefficient of $\log R_e$ obtained as 1.36 ± 0.26 which agrees well with the FP of early-type galaxies studied by (Jun & Im, 2008). They studied the wavelength dependence of coefficients in FP for cluster sample and reported the coefficient at 3.6μm observation was 1.55 ± 0.11.

Figure 4.4 shows the relation of Sérsic index and B/T with bulge structural parameters such as effective radius, mean surface brightness and bulge luminosity at 3.6μm.

The right hand side of Figure 4.4 shows galaxies defined as pseudobulges that had no correlation with Sérsic index and effective radius, mean surface brightness and bulge luminosity. Classical bulge galxies were less scattered than pseudobulges. Similar results were obtained for pseudobulges of early type galaxies studied in 3.6 μm wavelength by Fisher & Drory (2010). The different relations shown by the two categories of bulges with bulge structural parameters may be due to the difference in the distribution of stellar mass (Fisher & Drory, 2008, 2010).

Davari et al. (2017) reported that the disks of star-forming and quiescent galaxies evolve similarly, their bulges follow different evolutionary trajectories. The bulges present in an elliptical galaxy with disc could not be fitted like the bulges present in the elliptical galaxy without disc, because the Sérsic function that fits the bulges are less well constrained than elliptical (Fisher & Drory, 2010). Sérsic index need to be considered only one among the parameters to distinguish the types of bulges and in cases for which this criteria was not followed by the galaxies, other properties also need to be checked. Different parameters such as Sérsic index, morphology, star formation, kinematics (Kormendy, 1982), optical colour (Carollo et al., 1997; Fisher & Drory, 2010) and various scaling relations of structural parameters (Gadotti, 2009; Kormendy & Kennicutt, 2004; Fisher & Drory, 2010) could be used to understand the type of bulges present in galaxies. The morphologically identified pseudo bulges had active star formation (Fisher, 2006), with disc like morphology (Fabricius et al., 2012), and placed in different location of parameter space (Gadotti, 2009; Fisher & Drory, 2010).

Left hand side of the figure 4.4 shows the relation of B/T with bulge structural
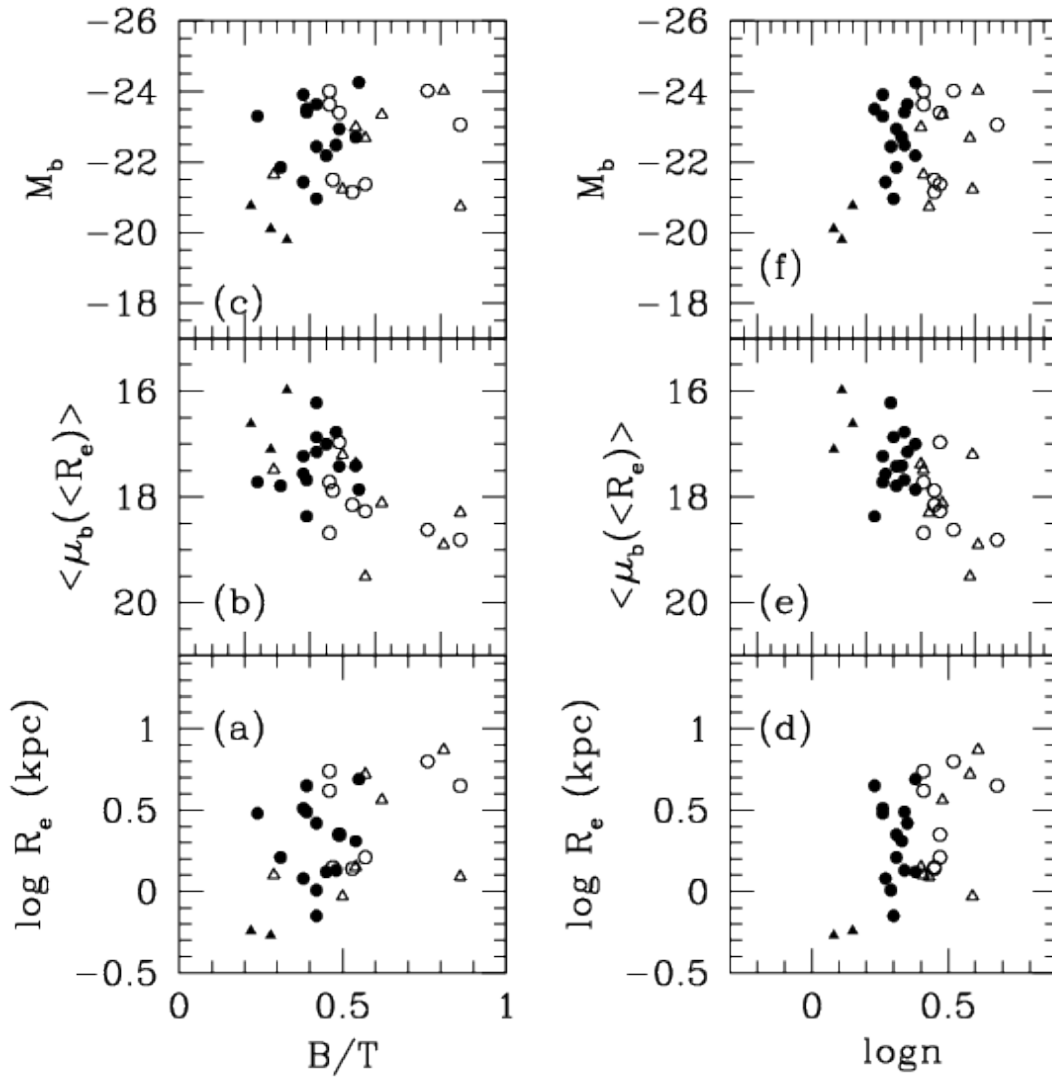
Figure 4.4: Relations of Sérsic index and B/T with bulge structural parameters. Open symbols represented as classical bulges and filled symbols represented as pseudo-bulges. R_e is the effective radius of the bulge, $<\mu_b(<R_e)>$ is effective surface brightness within R_e and M_b is the bulge luminosity.

parameters. The galaxies with larger bulge contribution had lower surface brightness. This is not a special case; the lower B/T values for pseudo-bulges represents disc dominated systems. The variation of B/T is due to the bulge component contribution (de Jong et al., 2004). So the lesser value of B/T had no detectable relation with bulge parameters of effective radius, surface brightness and luminosity .

4.4   Disc structural parameter correlations

The disc structural parameters of our sample galaxies were modeled by an exponential function. Figure 4.5 shows the disc structural parameter relations of classical and pseudo bulges. The disc luminosity and disc surface brightness were well related to the disc scale length. In Figure 4.5.a, the disc scale length was more for more luminous galaxies (r=-0.98) with lower central surface brightness (See Figure 4.5c).

In Figure 4.5c, we plot the disc central surface brightness as a function of disc scale length. The linear correlation was observed with 0.62. Galaxies with larger disc scale length had fainter surface brightness. Linear correlation coefficient between disc scale length and central surface brightness of pseudobulge galaxies was 0.72 with a significance of 99.78%. For galaxies with classical bulges, the correlation coefficient was 0.67 with the significance of 98.92%. Khosroshahi et al. (2000) found the relation (r=0.645) between the disc scale length and central brightness for early type spiral galaxies. Möllenhoff & Heidt (2001) reported that larger discs have lower disc central surface brightness for spirals galaxies in NIR observation and obtained the correlation (r=0.61). Bright ($M_T < -24.5$) and faint ($M_T > -24.5$) lenticular galaxies in NIR K- band were studied by Barway et al. (2009) and reported the similar relation. The bright lenticulars had large scatter compared to faint lenticulars. Vaghmare et al. (2013) studied the S0 galaxies in Mid-IR and observed that the galaxies with larger discs had fainter surface brightness, but for a given disc scale length the pseudo bulge hosting galaxies were fainter than the classical bulge hosting galaxies. There is a clear distinction between these two types of bulges. From the studies of pseudo bulges in different morphological types, Gadotti (2009) found that the disc scale length was more for galaxies with pseudo bulges with fainter surface brightness. But the relation of these two parameters of classical bulges and
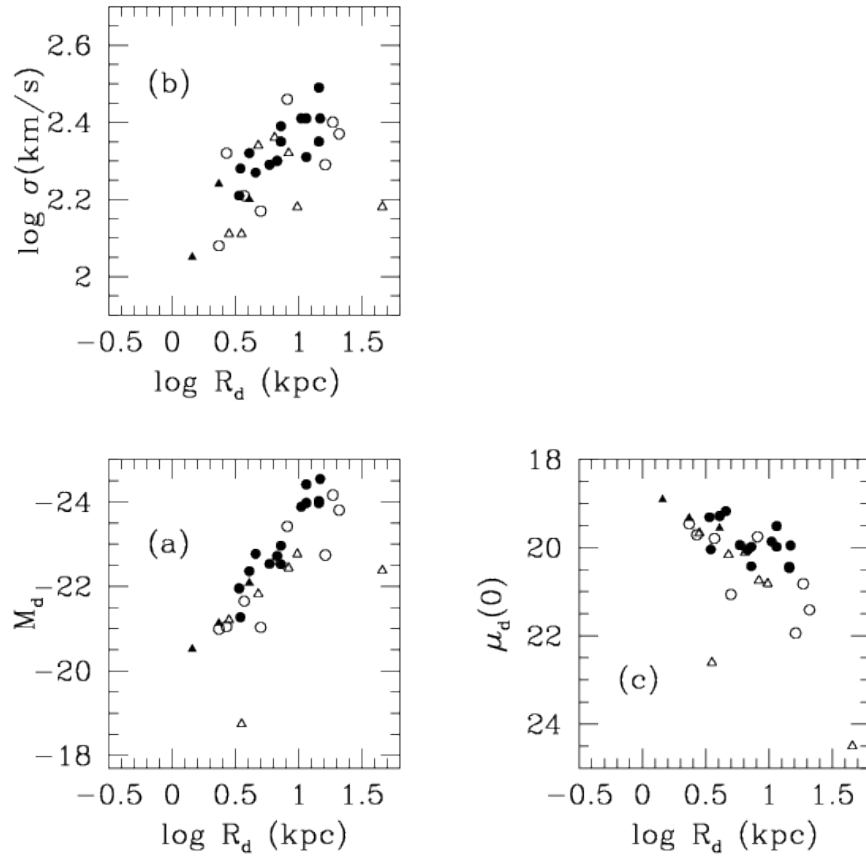
Figure 4.5: Relation between the disc structural parameters. (a) Size of the disc scae lengths are positively correlated to disc luminosity, (b) Correlation of disc scale length with veocity dispersion σ, suggested that larger the discs are resides in mssive systems and (c) Larger the size of the disc have lower the disc central surface brightness.

pseudo bulges overlap. Similarly in our study we have used early type galaxies, and we cannot distinct the classical and pseudo bulge galaxies from this relaion.

In Figure 4.5.b, the positive relation of disc scale length with velocity dispersion suggests that large discs are located in massive systems. Velocity dispersion is related to the virial mass of the bulge (Cappellari et al., 2006).
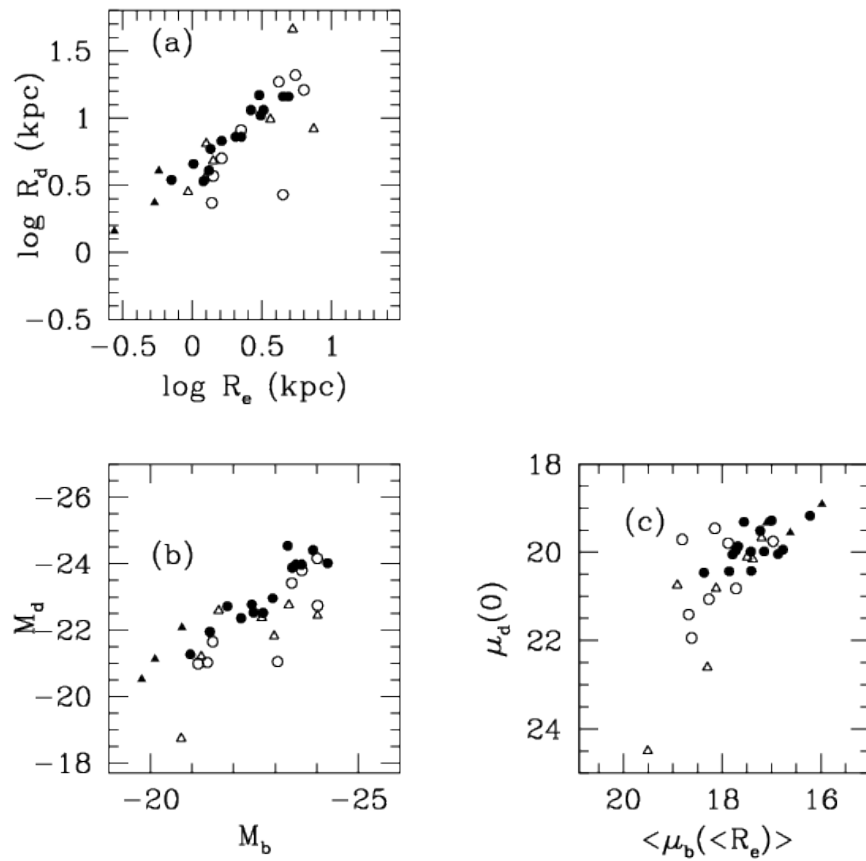
Figure 4.6: Relation between the bulge and disc structural parameters. Relation between the Effective radius R_e and disc scale length R_d(a), absolute luminosities(b) and Surface brightness(c).

4.5   Bulge disc correlations

In Figure 4.6 represents the relation between the bulge and disc structural components. The positive correlation between bulge effective radius and disc scale length (r= 0.87) shown in Figure 4.6a, indicates larger discs are found to be residing in larger bulges. This relation was first reported by (Courteau et al., 1996). Many of the studies reported that, formation of bulges in these galaxies from the disc through the secular evolution process (de Jong, 1996b; Möllenhoff & Heidt, 2001; MacArthur et al., 2003; Gadotti, 2009; Vaghmare et al., 2015). In the secular evolution model, the exponential disk was formed by the redistribution of angular momentum by viscous evolution, provided that star formation occurs on roughly the same timescale. The bulge formed naturally in such a model, and its properties depend only on the relative timescales of star formation and viscous transport and on the total angular momentum (Combes et al., 1990; Saio & Yoshii, 1990; Struck-Marcell, 1991).

In our sample, the pseudo bulges were well correlated than classical bulges. which indicates that larger discs are found in the larger galaxies. The correlation coefficient between effective radius and disc scale length of the pseudo bulge galaxies was found to be 0.95 with a significance >99.99%. In case of classical bulges the correlation coefficient was found to be 0.82 with a significance of 99.93%. Compared to pseudobulges the scatter was larger for classical bulges. This possibly implies the different formation mechanism on those galaxies. Barway et al. (2009) reported that there is a positive correlation of R_e and R_d observed in low luminosity galaxies supported the hypothesis that such galaxies formed by the stripping of gas from the halo and disk of late-type spiral galaxies, which formed their bulges through secular evolution. Anticorrelation of bulge effective radius and disc scale length was observed for their sample of more luminous lenticulars likely formed their bulges differently, possibly through a rapid collapse mechanism.

Absolute magnitude of bulge correlates well with that of disc as shown in Figure 4.6(b), which implies that large galaxies had more bulge, and more disc (de Jong, 1996b). Disc central surface brightness and effective surface brightness of bulge are also correlated, as shown in Figure 4.6(c).
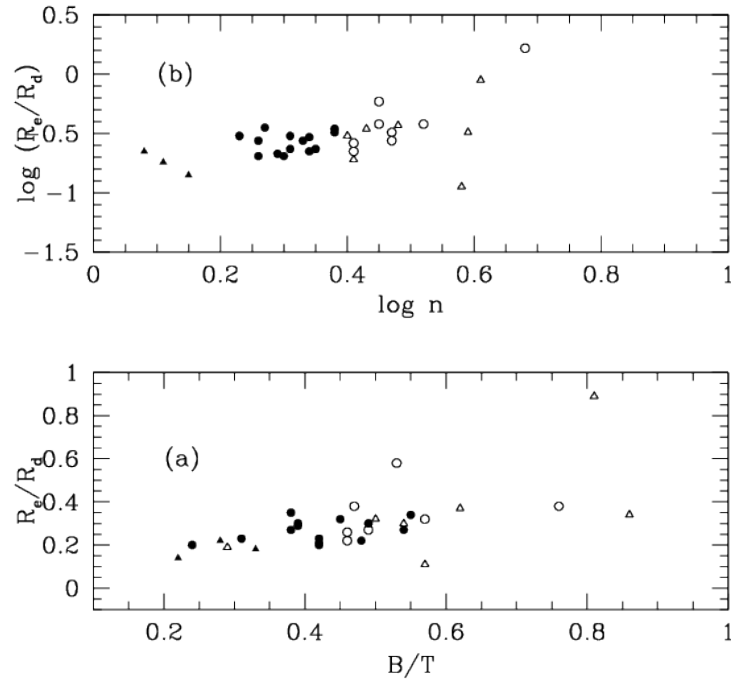
Figure 4.7: Relation between the ratio of R_e/R_d with Sérsic index and B/T

4.6   Relation of R_e/R_d with B/T

The ratio of bulge effective radius to disc scale length represented as R_e/R_d. This is mainly used to detect the relationship between the scale length of bulge and disc to Hubble type. The mean value of R_e/R_d of the whole sample from the Spitzer observations was 0.33. Courteau et al. (1996) studied the ratio of R_e/R_d for early type and late type spiral galaxies and obtained that early type spirals had lesser value of R_e/R_d ratio compared to late type spiral galaxies. It was supported by the findings of Graham & Prieto (1999). MacArthur et al. (2003) reported that this ratio would be less for late-type galaxies (early and late type spirals in K-band). Through the detailed bulge disc decomposition analysis of our sample, it was identified that a few of the sample galaxies behaved like classical bulges and hence the value as higher. Based on the separation of classical and pseudo bulges, we obtained the mean value of R_e/R_d for pseudo bulge galaxies as 0.25 and for classical bulges the value was found to be 0.44. Fisher & Drory (2008) studied the nature of pseudo

and classical bulges in optical data from HST and obtained seperate mean values of R_e/R_d for classical and pseudo bulges. The mean ratio of R_e/R_d for pseudo bulges and classical bulges were obtained as, 0.21±0.10 for pseudo bulges and 0.45±0.28 for classical bulges. In their sample they didnot obtain a correlation between effective radius and disc scale length for galaxies with classical bulge.

The concept of the scale free nature of Hubble type was studied by (Balcells et al., 2007; Laurikainen et al., 2007; Gadotti, 2009). Gadotti (2009) studied 1000 galaxies obtained from SDSS data and reported that Hubble sequence was not a scale free parameter. Hubble sequence depend on the scale length of the bulge and disc. Similar observations were obtained for Laurikainen et al. (2007) on the study of 216 disc galaxies of S0-Sm type in NIR images. The relation between R_e/R_d vs B/T of our sample were studied. Though the size of the sample was small, we identified a positive relation of B/T with R_e/R_d. From this relation, we could also strongly suggest that the Hubble sequence is not a scale free parameter and it depends on the bulge and disc sizes. Vika et al. (2014) studied the relation between these two parameters and observerd that a weak relation between these two parameters with large scatter was an indication of the dependency on morphological type. The difference in the relation of classical and pseudo bulges obtained in our sample strongly supports the formation of bulges via secular evolution. Scale length ratio was found to vary with Hubble type. This concept supported the hypothesis that more than one bulge formation mechanism may be at work. As suggested by Courteau et al. (1996), it may be possible that early-type and late-type disk galaxies were formed by different physical mechanisms, larger bulges formed principally from merger scenario and smaller bulges formed mainly via secular evolution (Khosroshahi et al., 2000).

We have obtained a positive relation between R_e/R_d and Sérsic index. We used the Sérsic index as the parameter to distinguish the nature of bulges. A good correlation with Sérsic index and R_e/R_d was found as shown in Figure 4.7.

4.7   Conclusion

Images obtained from Spitzer were analyzed by both isophotal fitting as well as by two dimensional bulge disc decomposition. From the two dimensional bulge disc decompostion analysis we obtained the bulge and disc structural parameters. From the image analysis, we identified few of the sample galaxies contain significant amount of disc component. The lower value of Sérsic index and B/T were present in our sample and was used to identify the significance of disc component.

The value of Sérsic index were used to divide the sample in to two groups. The value of n=2.5, the mean value of the distribution were used to seperate the sample into pseudobulges and classical bulges. Sérsic index $n<2.5$ characterises the galaxies with pseudo bulges and with $n>2.5$ characterises the nature of classical bulges. We found correlation of Sérsic index with B/T of the sample. Lesser value of Sérsic index galaxies which were identified as pseudobulges were well correlated than classical bulges. We also observed effective radius of pseudobulges as well correlated to disc scale length, while the classical bulges had scatter. The scale length of the disc was correlated with the size of its pseudobulge which strongly indicate the different physical mechanism in different bulge type Fisher & Drory (2008). In all relations shown in Figure 4.3, we found that there was a clear distinction between the bulge types. We also found the ratio of R_e/R_d of pseudobulges as consistent with MacArthur et al. (2003) and Fisher & Drory (2008). Correlations of R_e/R_d with B/T and n suggested that pseudobulges were built by secular evolution. The simplest mechanism controlling the Sérsic index in bulges was that Sérsic index grows with time as the bulge to total ratio increases. Otherwise Sérsic index n in a pseudobulges were time dependent quantity. It is well known that lenticular galaxies contained disc component. However, the interesting part of the study is the presence of significant disc component in elliptical galaxies. In our analysis it was infered that in case of significant disc component, the lenticulars as well as ellipticals behave like pseudobulge galaxies. Though for lenticulars the presence of pseudo bulge is common, it is curious in case of ellipticals galaxies.

So we expect the galaxies with pseudo bulges would not follow the same formation scenarios of normal ellipticals. The bulges formed in these galaxies are from

the already existing disc via secular evolution process.

In the next chapter, we summarise the results obtained from the NIR and Mid-IR photometric analysis. Future plan is also discussed thereafter.

Chapter 5

Summary and future plans

5.1 Summary

The main objective of the thesis was morphological analysis of early-type galaxies. We focussed on photometric structural analysis on nearby early-type galaxies observed in near infrared (2.16μm) and mid infrared (3.6μm) wavelengths. Chapter 1 provide introduction about the galaxies explaining their morphological classification and mentioned the different formation scenarios of galaxies. The possibilities of the existence of different types of bulges such as classical or pseudo-bulges in the galaxy were also discussed. Photometric structural analysis techniques were used for this study. As a preliminary step, usual surface photometry techniques of isophotal fitting were done and detailed analysis was carried out by two dimensional bulge disc decomposition.

The selected sample contained 65 nearby early type galaxies with 45 ellipticals and 20 lenticulars. Distinct properties of the sample were that, all of them had ionised gas and resides in a low density environment. The near infrared images of 54 galaxies were available from Two Micron All Sky Survey (2MASS) and mid infrared images of 39 galaxies were available from Spitzer observations. Fitting the elliptical isophotes on the images of galaxies was done with the help of a software package IRAF/stsdas with the task *ellipse*. Two dimensional image analysis was done on each of the images with the help of the algorithm GALFIT. Central spheroidal component of the galaxies was modeled by Sérsic function and outer disc component by

exponential function. By this modeling we could extract the structural components of bulge, disc and their parameters. The magnitudes, ellipticity, position angle of bulge and disc components were obtained besides the effecive radius and disc scale length.

Out of the 65 galaxies, 54 were available from 2MASS observation and were studied at J (1.25 μm) and K (2.2μm) band images. The correlation analysis of structural parameters mainly focussed on K-band observational data. In NIR, K-band observations had very little dust extinction and also would be sensitive to older stellar populations. It favoured to identify the structural components in this waveband than optical. Hence effect of recent star formation activities was reduced in the galaxy images. By two dimensional image analysis we obtained average value of Sérsic index 1.18 ± 0.21 and B/T ratio (mean value as 0.32 ± 0.07). The relations between the structural parameters of bulge and disc were also analysed. Larger galaxies were more luminous and had fainter surface brightness. The well known scaling relations of Kormendy relation for our sample (linear correlation coefficient $r = 0.66$) was comparable to that of Coma ellipticals. The three parameter correlation of Fundamental Plane showed similar slopes when compared to Coma cluster ellipticals. Other correlations of bulge structural parameters were not observed. The disc structural parameters such as disc scale length, central surface brightness and disc luminosity were also analysed. The galaxies which were more luminous had larger disc scale length and had fainter central surface brightness. The interesting result observed from this 2MASS image analysis was the relation between effective radius of bulge and disc scale length. The positive correlation of bulge and disc parameters of size, luminosity and surface brightness pointed out the formation of bulges from the already existing disc component. Such type of bulges would be formed via secular evolution process. Similar coefficient obtained for KR and FP relation of our early type sample with cluster sample, point out that the same formation scenarios would be followed for cluster and our sample. Considering the shallowness of 2MASS images, analysis was also carried out with deeper images from spitzer to endorse our findings.

39 out of 54 have Spitzer observations. Preliminary reduction was completed

with the help of MOPEX software. Detailed image analysis was carried out by two dimensional bulge disc decomposition. From the extracted parameters, positive correlation of Sérsic index and B/T was observed (linear correlation as r=0.61). The total sample was divided into two groups based on the Sérsic index (mean value of n=2.5). Lower value of Sérsic index (n <2.5) represented a set of galaxies dominated by pseudo-bulges and higher value of Sérsic index (n>2.5) represented classical bulges. Sérsic index and B/T of pseudo bulges were not related to the bulge structural parameters (see Figure 4.4) whereas these were related in the classical bulges. Different relations were shown in pseudo bulges and classical bulges with bulge structural parameters. These two categories of bulges are structurally distinct due to the difference in the distribution of stellar mass.

The scaling relation of Kormedy relation for pseudo-bulges and classical bulges were analysed and obtained similar slopes (see Section 4.3). The coefficients of FP relation were similar with the literature of mid-infrared FP for early-type galaxies of cluster sample.

The disc structural parameters of classical and pseudo bulges were studied. The disc parameters of pseudo bulges were well correlated as compared to classical bulges. The positive relation with velocity dispersion and disc scale length suggested that, larger discs reside in massive galaxies or massive bulges, since the velocity dispersion was related to the virial mass of the bulge. The relation between disc scale length of pseudo bulges and classical bulges with luminosity were studied. The classical bulge galaxies were found as more scattered compared to pseudo bulges in this relation.

The correlation between the bulge and disc structural parameters were studied and infered that larger discs reside in galaxies with larger bulges. In case of luminosity also it was well correlated. The classical bulges were scattered more compared to pseudo bulges. Since these two bulge types were structurally different, we infer that they would have different formation scenarios.

Our findings along with major observations identified through the analysis are concluded as follows,

- All elliptical galaxies are not single component systems, and may contain

smaller or larger discs. The quantitative structural analysis in multi wavelength observations could help to identify the hidden component present in such galaxies.

- Different types of bulges were present in our sample galaxies which were identified by the lower value of Sérsic index. The galaxies with lower value of Sérsic index (n <2.5) behave like pseudo-bulges and Sérsic index (n >2.5) like classical bulges.

- The significant disc component was observed in sample galaxies including elliptical galaxies.

- Difference in the relation of pseudo-bulges and classical bulges with structural parameters suggests that different formation scenarios would exist for such galaxies even if they exhibit various similar properties.

- The positive correlation of effective radius and disc scale length observed in both the studies pointed out that larger discs reside in larger galaxies. This inference supports that the formation of bulges present in those galaxies may be from already existing disc via secular evolution.

5.2 Future plan:

The studies on the structural analysis of nearby early-type galaxies in Infrared waveband paves way for future research on the same as stated below.

- Very few attempts were observed in the structural studies on nearby field ellipticals in mid-infrared. A quantitative structural study in multi wavelength on field elliptical galaxies could help to reveal the different structures present in these systems.

- The kinematics of stars in bulge and disc could also be analysed which may lead to identify the presence of young stars in the central region.

Bibliography

Abhyankar, K. D. 1992, Astrophysics Stars and Galaxies

Andredakis, Y. C., Peletier, R. F., & Balcells, M. 1995, MNRAS, 275, 874

Annibali, F., Bressan, A., Rampazzo, R., Zeilinger, W. W., & Danese, L. 2007, A&A, 463, 455

Annibali, F., Bressan, A., Rampazzo, R., et al. 2010, A&A, 519, A40

Arp, H. 1966, ApJS, 14, 1

Athanassoula, E. 2005, MNRAS, 358, 1477

Balcells, M., Graham, A. W., & Peletier, R. F. 2007, ApJ, 665, 1104

Barway, S., Wadadekar, Y., Kembhavi, A. K., & Mayya, Y. D. 2009, MNRAS, 394, 1991

Bender, R., & Moellenhoff, C. 1987, A&A, 177, 71

Bender, R., Surma, P., Doebereiner, S., Moellenhoff, C., & Madejsky, R. 1989, A&A, 217, 35

Bernardi, M., Sheth, R. K., Annis, J., et al. 2003, AJ, 125, 1817

Bertin, E., & Arnouts, S. 1996, A&AS, 117, 393

Binney, J., & Merrifield, M. 1998, Galactic Astronomy

Blackman, C. P., Axon, D. J., & Taylor, K. 1979, MNRAS, 189, 751

Bournaud, F., Perret, V., Renaud, F., et al. 2014, ApJ, 780, 57

Boylan-Kolchin, M., Ma, C.-P., & Quataert, E. 2006, MNRAS, 369, 1081

Bressan, A., Chiosi, C., & Fagotto, F. 1994, ApJS, 94, 63

Buta, R. J. 2011, ArXiv e-prints

Byun, Y. I., & Freeman, K. C. 1995, ApJ, 448, 563

Caon, N., Capaccioli, M., & D'Onofrio, M. 1993, MNRAS, 265, 1013

Cappellari, M., Bacon, R., Bureau, M., et al. 2006, MNRAS, 366, 1126

Carollo, C. M. 1999, ApJ, 523, 566

Carollo, C. M., Franx, M., Illingworth, G. D., & Forbes, D. A. 1997, ApJ, 481, 710

Combes, F., Debbasch, F., Friedli, D., & Pfenniger, D. 1990, A&A, 233, 82

Conselice, C. J., Mortlock, A., Bluck, A. F. L., Grützbauch, R., & Duncan, K. 2013, MNRAS, 430, 1051

Courteau, S., de Jong, R. S., & Broeils, A. H. 1996, ApJ, 457, L73

Davari, R. H., Ho, L. C., Mobasher, B., & Canalizo, G. 2017, ApJ, 836, 75

Davis, L. E., Cawson, M., Davies, R. L., & Illingworth, G. 1985, AJ, 90, 169

de Carvalho, R. R., & Djorgovski, S. 1992, ApJ, 389, L49

de Jong, R. S. 1996a, A&AS, 118, 557

—. 1996b, A&A, 313, 45

de Jong, R. S., Simard, L., Davies, R. L., et al. 2004, MNRAS, 355, 1155

de Souza, R. E., Gadotti, D. A., & dos Anjos, S. 2004, ApJS, 153, 411

de Vaucouleurs, G. 1948, Annales d'Astrophysique, 11, 247

—. 1953, MNRAS, 113, 134

—. 1977, ApJS, 33, 211

—. 1991, Science, 254, 1053

Desroches, L.-B., Quataert, E., Ma, C.-P., & West, A. A. 2007, MNRAS, 377, 402

Djorgovski, S., & Davis, M. 1987, ApJ, 313, 59

D'Onofrio, M., Capaccioli, M., Merluzzi, P., Zaggia, S., & Boulesteix, J. 1999, A&AS, 134, 437

Dressler, A. 1980, ApJS, 42, 565

—. 1984, ApJ, 281, 512

Dressler, A., Lynden-Bell, D., Burstein, D., et al. 1987, ApJ, 313, 42

Durbala, A., Sulentic, J. W., Buta, R., & Verdes-Montenegro, L. 2008, MNRAS, 390, 881

Eggen, O. J., Lynden-Bell, D., & Sandage, A. R. 1962, ApJ, 136, 748

Emsellem, E., & Arsenault, R. 1997, A&A, 318, L39

Emsellem, E., Cappellari, M., Krajnović, D., et al. 2011, MNRAS, 414, 888

Faber, S. M. 1973, A&AS, 10, 201

Faber, S. M., & Jackson, R. E. 1976, ApJ, 204, 668

Fabricius, M. H., Saglia, R. P., Fisher, D. B., et al. 2012, ApJ, 754, 67

Falcón-Barroso, J., van de Ven, G., Peletier, R. F., et al. 2011, MNRAS, 417, 1787

Fazio, G. G., Hora, J. L., Allen, L. E., et al. 2004, ApJS, 154, 10

Fernández Lorenzo, M., Sulentic, J., Verdes-Montenegro, L., et al. 2014, ApJ, 788, L39

Fish, R. A. 1964, ApJ, 139, 284

Fisher, D. B. 2006, ApJ, 642, L17

Fisher, D. B., & Drory, N. 2008, AJ, 136, 773

—. 2010, ApJ, 716, 942

Forbes, D. A., Ponman, T. J., & Brown, R. J. N. 1998, ApJ, 508, L43

Freeman, K. C. 1970, ApJ, 160, 811

Gadotti, D. A. 2008, MNRAS, 384, 420

—. 2009, MNRAS, 393, 1531

Gallazzi, A., Charlot, S., Brinchmann, J., White, S. D. M., & Tremonti, C. A. 2005, MNRAS, 362, 41

Gao, J., Jiang, B. W., & Li, A. 2009, ApJ, 707, 89

Genzel, R., Burkert, A., Bouché, N., et al. 2008, ApJ, 687, 59

Graham, A. W. 2001, AJ, 121, 820

Graham, A. W., & Prieto, M. 1999, Ap&SS, 269, 653

Hubble, E., & Sandage, A. 1953, ApJ, 118, 353

Hubble, E. P. 1926, ApJ, 64

—. 1936, Realm of the Nebulae

Jarrett, T. H., Chester, T., Cutri, R., et al. 2000, AJ, 119, 2498

Jarrett, T. H., Chester, T., Cutri, R., Schneider, S. E., & Huchra, J. P. 2003, AJ, 125, 525

Jedrzejewski, R. I. 1987, MNRAS, 226, 747

Jiang, F.-Z., Huang, S., & Gu, Q.-S. 2011, Research in Astronomy and Astrophysics, 11, 309

Jorgensen, I., & Franx, M. 1994, ApJ, 433, 553

Jorgensen, I., Franx, M., & Kjaergaard, P. 1996, MNRAS, 280, 167

Jun, H. D., & Im, M. 2008, ApJ, 678, L97

Kampakoglou, M., Trotta, R., & Silk, J. 2008, MNRAS, 384, 1414

Kauffmann, G. 1996, MNRAS, 281, 487

Kauffmann, G., & Charlot, S. 1998, MNRAS, 294, 705

Kennicutt, Jr., R. C. 1981, AJ, 86, 1847

Khosroshahi, H. G., Wadadekar, Y., & Kembhavi, A. 2000, ApJ, 533, 162

Kormendy, J. 1977, ApJ, 218, 333

—. 1982, Morphology and dynamics of galaxies; Proceedings of the Twelfth Advanced Course, Saas-Fee, Switzerland, March 29-April 3, 1982 (A84-15502 04-90). Sauverny, Switzerland, Observatoire de Geneve, 1983, p. 113-288., 12, 113

Kormendy, J., & Bruzual A., G. 1978, ApJ, 223, L63

Kormendy, J., & Kennicutt, Jr., R. C. 2004, ARA&A, 42, 603

Krajnović, D., Emsellem, E., Cappellari, M., et al. 2011, MNRAS, 414, 2923

Kuntschner, H., Smith, R. J., Colless, M., et al. 2002, MNRAS, 337, 172

La Barbera, F., de Carvalho, R. R., de La Rosa, I. G., & Lopes, P. A. A. 2010, MNRAS, 408, 1335

La Barbera, F., Merluzzi, P., Massarotti, M., Busarello, G., & Capaccioli, M. 2003, Mem. Soc. Astron. Italiana, 74, 478

Larson, R. B., Tinsley, B. M., & Caldwell, C. N. 1980, ApJ, 237, 692

Laurikainen, E., Salo, H., & Buta, R. 2005, MNRAS, 362, 1319

Laurikainen, E., Salo, H., Buta, R., & Knapen, J. H. 2007, MNRAS, 381, 401

Laurikainen, E., Salo, H., Buta, R., Knapen, J. H., & Comerón, S. 2010, MNRAS, 405, 1089

Liu, F.-S., Deng, Z.-G., Wu, H., & Xia, X.-Y. 2008, Chinese J. Astron. Astrophys., 8, 503

MacArthur, L. A., Courteau, S., & Holtzman, J. A. 2003, ApJ, 582, 689

Malin, D. F., & Carter, D. 1983, ApJ, 274, 534

Méndez-Abreu, J., Simonneau, E., Aguerri, J. A. L., & Corsini, E. M. 2010, A&A, 521, A71

Michard, R. 1985, A&AS, 59, 205

Milvang-Jensen, B., & Jørgensen, I. 1999, Baltic Astronomy, 8, 535

Mobasher, B., Guzman, R., Aragon-Salamanca, A., & Zepf, S. 1999, MNRAS, 304, 225

Möllenhoff, C., & Heidt, J. 2001, A&A, 368, 16

Naab, T., & Burkert, A. 2001, ApJ, 555, L91

Noordermeer, E., & van der Hulst, J. M. 2007, MNRAS, 376, 1480

Pahre, M. A., de Carvalho, R. R., & Djorgovski, S. G. 1998, AJ, 116, 1606

Pahre, M. A., Djorgovski, S. G., & de Carvalho, R. R. 1995, ApJ, 453, L17

Paturel, G., Petit, C., Prugniel, P., et al. 2003, VizieR Online Data Catalog, 7237

Peng, C. Y., Ho, L. C., Impey, C. D., & Rix, H.-W. 2002, AJ, 124, 266

—. 2010, AJ, 139, 2097

Postman, M., Franx, M., Cross, N. J. G., et al. 2005, ApJ, 623, 721

Rauscher, B. J., Lloyd, J. P., Barnaby, D., et al. 1998, ApJ, 506, 116

Ravikumar, C. D., Barway, S., Kembhavi, A., Mobasher, B., & Kuriakose, V. C. 2006, A&A, 446, 827

Reda, F. M., Forbes, D. A., Beasley, M. A., O'Sullivan, E. J., & Goudfrooij, P. 2004, MNRAS, 354, 851

Reda, F. M., Forbes, D. A., & Hau, G. K. T. 2005, MNRAS, 360, 693

Renzini, A. 2006, ARA&A, 44, 141

Reynolds, J. H. 1913, MNRAS, 74, 132

Rix, H.-W., & White, S. D. M. 1990, ApJ, 362, 52

Roberts, M. S., Hogg, D. E., Bregman, J. N., Forman, W. R., & Jones, C. 1991, ApJS, 75, 751

Saio, H., & Yoshii, Y. 1990, ApJ, 363, 40

Salo, H., Laurikainen, E., Laine, J., et al. 2015, ApJS, 219, 4

Samir, R. M., Reda, F. M., Shaker, A. A., Osman, A. M. I., & Amin, M. Y. 2016, NRIAG Journal of Astronomy and Geophysics, 5, 277

Sandage, A., & Tammann, G. A. 1987, A revised Shapley-Ames Catalog of bright galaxies

Sandage, A., & Visvanathan, N. 1978, ApJ, 225, 742

Schombert, J., & Smith, A. K. 2012, PASA, 29, 174

Scorza, C., & van den Bosch, F. C. 1998, MNRAS, 300, 469

Sérsic, J. L. 1963, Boletin de la Asociacion Argentina de Astronomia La Plata Argentina, 6, 41

Sersic, J. L. 1968, Atlas de galaxias australes

Simard, L. 1998, in Astronomical Society of the Pacific Conference Series, Vol. 145, Astronomical Data Analysis Software and Systems VII, ed. R. Albrecht, R. N. Hook, & H. A. Bushouse, 108

Skrutskie, M. F., Cutri, R. M., Stiening, R., et al. 2006, AJ, 131, 1163

Struck-Marcell, C. 1991, ApJ, 368, 348

Tantalo, R., Chinellato, S., Merlin, E., Piovan, L., & Chiosi, C. 2010, A&A, 518, A43

Terlevich, A. I., & Forbes, D. A. 2002, MNRAS, 330, 547

Terlevich, A. I., Kuntschner, H., Bower, R. G., Caldwell, N., & Sharples, R. M. 1999, MNRAS, 310, 445

Tortora, C., Pipino, A., D'Ercole, A., Napolitano, N. R., & Matteucci, F. 2013, MNRAS, 435, 786

Tully, R. B. 1988, AJ, 96, 73

Vaghmare, K., Barway, S., & Kembhavi, A. 2013, ApJ, 767, L33

Vaghmare, K., Barway, S., Mathur, S., & Kembhavi, A. K. 2015, MNRAS, 450, 873

Väisänen, P., Morel, T., Rowan-Robinson, M., et al. 2002, MNRAS, 337, 1043

van der Kruit, P. C. 1987, A&A, 173, 59

Vika, M., Bamford, S. P., Häußler, B., & Rojas, A. L. 2014, MNRAS, 444, 3603

Visvanathan, N., & Sandage, A. 1977, ApJ, 216, 214

Wadadekar, Y., Robbason, B., & Kembhavi, A. 1999, AJ, 117, 1219

Weinzirl, T., Jogee, S., Khochfar, S., Burkert, A., & Kormendy, J. 2009, ApJ, 696, 411

Wyse, R. F. G., Gilmore, G., & Franx, M. 1997, ARA&A, 35, 637

Zepf, S. E., & Whitmore, B. C. 1993, ApJ, 418, 72